

1 **Primary and secondary emissions from a modern fleet of city buses**
2 **Online characterization of primary and secondary emissions of**
3 **particulate matter and acidic molecules from a modern fleet of city**
4 **buses**

5 Liyuan Zhou^{1,2#}, Qianyun Liu^{2,a#}, Christian M. Salvador^{3,b}, Michael Le Breton^{3,c}, Mattias Hallquist³, Jian
6 Zhen Yu⁴ and Chak K. Chan^{1,2*}, Åsa M. Hallquist^{5*}

7
8 ¹ Division of Physical Sciences and Engineering, King Abdullah University of Science and Technology, Thuwal, Saudi Arabia

9 ² School of Energy and Environment, City University of Hong Kong, Hong Kong SAR, China

10 ³ Department of Chemistry and Molecular Biology, University of Gothenburg, Gothenburg, Sweden

11 ⁴ Division of Environment and Sustainability, Hong Kong University of Science and Technology, Hong Kong, China

12 ⁵ IVL Swedish Environmental Research Institute, Gothenburg, Sweden

13 ^anow at: RELX Science Center, Shenzhen RELX Tech. Co., Ltd., Shenzhen, China

14 ^bnow at: Environmental Sciences Division, Oak Ridge National Laboratory, Oak Ridge, TN 37830, USA

15 ^cnow at: FEV Sverige AB, Gothenburg, Sweden

16

17

18 #The authors contribute equally.

19 *Correspondence to:* Åsa M Hallquist (asa.hallquist@ivl.se); Chak K. Chan (chak.chan@kaust.edu.sa)

20

21 **Abstract.** The potential impact of transitioning from conventional fossil fuel to a non-fossil fuel vehicle fleet was investigated
22 by measuring primary emissions via extractive sampling of bus plumes and assessing secondary mass formation using a
23 Gothenburg Potential Aerosol Mass (Go:PAM) reactor from 76 in-use transit buses. Online chemical characterization of
24 gaseous and particulate emissions from these buses was conducted using a chemical ionization mass spectrometry (CIMS)
25 with acetate as the reagent ion, coupled with a filter inlet for gases and aerosols (FIGAERO). Acetate reagent ion chemistry
26 selectively ionizes acidic compounds, including organic and inorganic acids, as well as nitrated and sulfated organics. A
27 significant reduction (48-98%) in fresh particle emissions was observed in buses utilizing compressed natural gas (CNG),
28 biodiesels like rapeseed methyl ester (RME) and hydrotreated vegetable oil (HVO), as well as hybrid-electric HVO (HVO_{HEV}),
29 compared to diesel (DSL) buses. However, secondary particle formation from photooxidation of emissions was substantial
30 across all fuel types. The median ratio of particle mass emission factors of aged to fresh emissions increased in the following
31 order: DSL buses at 4.0, HVO buses at 6.7, HVO_{HEV} buses at 10.5, RME buses at 10.8, and CNG buses at 84. Of the compounds
32 that can be identified by CIMS, fresh gaseous emissions from all Euro V/EEV buses, regardless of fuel type, were dominated
33 by nitrogen-containing compounds such as nitrous acid (HONO), nitric acid (HNO₃), and isocyanic acid (HNCO), alongside
34 small monoacids (C₁-C₃). Notably, nitrogen-containing compounds were significantly reduced in Euro VI buses-the emission

35 of nitrogen-containing compounds was notably lower in Euro VI buses equipped with more advanced emission control
36 technologies. Secondary gaseous organic acids correlated strongly with gaseous HNO₃ signals (R²= 0.85-0.99) in Go:PAM,
37 but their moderate to weak correlations with post-photooxidation secondary particle mass suggest they are not reliable tracers
38 for secondary organic aerosol formation from bus exhaust. Our study highlights that non-regulated compounds and secondary
39 pollutant formation, not currently addressed in legislation, are crucial considerations in the evaluation of environmental
40 impacts of future fuel and engine technology shifts.

41 **1. Introduction**

42 Air pollution remains a critical global issue, posing significant threats to both human health and the environment. Despite
43 substantial progress in reducing emissions from major sources like industry, energy production, households, transportation,
44 and agriculture, the worldwide achievement of air quality targets continues to be a daunting challenge. Notably, the road
45 transport sector, particularly in urban environments, significantly contributes to the emissions of nitrogen oxides (NO_x) and
46 particulate matter (PM), impacting the health of individuals in densely populated regions. In tandem with these concerns,
47 efforts to combat climate change have spurred an increase in the adoption of renewable energy sources within the transportation
48 sector. Biodiesel has risen as the most prevalent renewable fuel, followed by biogas and ED95 ethanol (Guerreiro et al., 2014).
49 Moreover, numerous cities are progressively integrating hybrid-electric and electric vehicles into their public transport fleets,
50 aiming to reduce emissions.

51
52 Emissions from vehicles, especially buses, exhibit considerable variability. They are influenced by fuel type, engine design,
53 operational conditions, emission after-treatment technologies and maintenance (Pirjola et al., 2016; Zhao et al., 2018; Watne
54 et al., 2018; Liu et al., 2019a; Zhou et al., 2020). While diesel (DSL) buses are common, there is an increasing trend towards
55 the use of alternative fuels such as compressed natural gas (CNG), rapeseed methyl ester (RME), and hydrotreated vegetable
56 oil (HVO). These alternative fuels offer several benefits, including reduced PM emissions, particularly soot, and lower levels
57 of carbon monoxide (CO) and total hydrocarbons (THC) (Pflaum et al., 2010; Hassaneen et al., 2012; Liu et al., 2019a).
58 However, the efficacy of RME and HVO in diminishing NO_x emissions can be inconsistent (Pirjola et al., 2016; Liu et al.,
59 2019a); and CNG buses exhibit considerable variability in particle number (PN) emissions (Watne et al., 2018). In Sweden,
60 approximately 23% of the fuel mix of the transport sector in 2020 comprised renewable fuels, with HVO accounting for over
61 half of this proportion (Vourliotakis and Platsakis, 2022; Energimyndigheten, 2021). Emission control strategies, such as
62 aftertreatment systems including diesel particulate filters (DPFs) and selective catalytic reduction (SCR) systems, have been
63 implemented to mitigate pollutant emissions from vehicles. These systems have shown significant efficacy in reducing PM
64 and NO_x emissions respectively, though their performance can vary under different operational conditions.

65

66 ~~Accurately determining vehicle emission factors (EFs) is essential for developing and implementing effective air quality~~
67 ~~policies (Fitzmaurice and Cohen, 2022). Various methodologies, including testing cycles, on-road chasing, and portable~~
68 ~~emission measurement systems (PEMS), have been employed to measure vehicle emissions (Kwak et al., 2014; Jezek et al.,~~
69 ~~2015; Pirjola et al., 2016). Roadside or near-road measurements of on-road vehicle emissions provide a larger sample size in~~
70 ~~a shorter timeframe, which is especially relevant for estimating the exposure of pedestrians and bus passengers. In a prior~~
71 ~~study, we reported EFs for general air pollutants such as PM, NO_x, CO, and THC from individual buses in an in-use bus fleet,~~
72 ~~based on stop-and-go measurements at a bus stop in Gothenburg, Sweden (Liu et al., 2019a). Our findings indicated that~~
73 ~~hybrid buses, when using their combustion engines to accelerate from a standstill at bus stops, tended to emit higher particle~~
74 ~~numbers (PN) than traditional DSL buses, likely due to their relatively smaller engines.~~

75
76 Accurately determining vehicle emission factors (EFs) is crucial for devising and implementing effective air quality
77 policies (Fitzmaurice and Cohen, 2022). Methods such as chassis dynamometer tests, on-board measurements with portable
78 emission measurement systems (PEMS), and on-road vehicle chasing experiments have been employed to assess emissions
79 from various types of vehicles (Kwak et al., 2014; Jezek et al., 2015; Pirjola et al., 2016). Chassis dynamometer tests offer
80 high repeatability over standard drive cycles but may not reflect real-world driving conditions or fleet maintenance levels.
81 There are also challenges in accurately replicating real-world dilution effects (Vogt et al., 2003; Kuitinen et al., 2021). On-
82 board measurements with PEMS provide data under a wide range of operating conditions, yet like dynamometers, they may
83 not realistically mimic ambient dilution processes (Giechaskiel et al., 2015; Wang et al., 2020). On-road vehicle chasing
84 experiments involve following individual vehicles with a mobile laboratory to capture the exhaust plumes, providing insights
85 into realistic dilution processes from the tailpipe to ambient air, though these experiments often require a test track to ensure
86 traffic safety (Wang et al., 2020; Tong et al., 2022). All three methods are limited by small sample sizes, which constrain
87 understanding of the real emission characteristics of vehicle fleets. Alternatively, roadside or near-road measurements provide
88 the ability to monitor emissions from a large number of vehicles under actual driving conditions within a short
89 timeframe (Hallquist et al., 2013; Watne et al., 2018; Liu et al., 2019a), which is particularly important for assessing exposure
90 risks to pedestrians and bus passengers. However, this method is limited by its inability to monitor specific engines or
91 operational conditions, such as varying engine speeds and loads. Integrating results from diverse methodologies would ideally
92 yield a comprehensive understanding of emissions from vehicle transport systems.

93
94 ~~Primary emissions are not the only way in which engine emissions impact air quality. Emissions from engine exhaust can~~
95 ~~contribute to secondary particles through oxidation of gas phase species, primarily via functionalization reactions, yielding~~
96 ~~lower volatility products (Hallquist et al., 2009; Kroll et al., 2009). Laboratory studies have demonstrated that the amount of~~
97 ~~secondary organic aerosols (SOA) produced from diluted vehicle exhaust frequently surpasses that of primary organic aerosols~~
98 ~~(POA) within less than one day of atmospheric equivalent aging (Nordin et al., 2013; Platt et al., 2013; Gordon et al., 2014b;~~
99 ~~Liu et al., 2015; Chirico et al., 2010). In addition, primary emissions may also be oxidized to higher volatility products via~~

100 fragmentation reactions. Engine exhaust is a recognized primary source of organic acids in the atmosphere (Friedman et al.,
101 2017), and the oxidation of hydrocarbons from the exhaust by hydroxyl radicals (OH) results in a diverse array of products
102 with numerous functional groups, including carboxylic acids ($-COOH$) (Yao et al., 2002). However, the secondary production
103 of organic acid from engine exhaust remains poorly characterized, and it may significantly contribute to the overall organic
104 acid budget and help explain discrepancies between models and measurements (Millet et al., 2015; Yuan et al., 2015; Paulot
105 et al., 2011). Recent development of analytical techniques has enabled tools for simultaneous online measurements of gas and
106 particle phase species at a high time resolution by utilizing a high-resolution time-of-flight chemical ionization mass
107 spectrometry (HR-ToF-CIMS) coupled with a filter inlet for gases and aerosols (FIGAERO) (Le Breton et al., 2019; Friedman
108 et al., 2017; Lopez-Hilfiker et al., 2014; Zhou et al., 2021). Oxidation flow reactors (OFRs) enable the simulation of several
109 days of atmospheric aging in a few minutes, with minimized wall effects compared to traditional smog chamber
110 experiments (Palm et al., 2016; Bruns et al., 2015). OFRs have been utilized in numerous studies to investigate the SOA
111 potential of ambient air and emissions from different sources, including motor exhausts (Simonen et al., 2017; Kuittinen et
112 al., 2021; Bruns et al., 2015; Tkacik et al., 2014; Watne et al., 2018; Liu et al., 2019b; Yao et al., 2022; Zhou et al., 2021). For
113 real-world traffic measurement studies using point sampling, OFRs with short response times enable the investigation of a
114 large number of vehicles, thus capturing the large variability between individual vehicles in a fleet (Watne et al., 2018; Zhou
115 et al., 2021; Liao et al., 2021b; Ghadimi et al., 2023).

116
117 In a prior study, we conducted roadside point measurements and reported EFs for general air pollutants such as PM, NO_x, CO,
118 and THC from individual buses during stop-and-go operations at a bus stop in Gothenburg, Sweden (Liu et al., 2019a). Our
119 findings showed that hybrid buses, when using their combustion engines to accelerate from a standstill at bus stops, tended to
120 emit higher particle numbers (PN) than traditional DSL buses, likely due to their relatively smaller engines. Expanding on our
121 prior findings, it is important to acknowledge that primary emissions are not the only way in which engine emissions impact
122 air quality. Emissions from engine exhaust can contribute to secondary particles through oxidation of gas-phase species,
123 primarily via functionalization reactions, yielding lower-volatility products (Hallquist et al., 2009; Kroll et al., 2009).
124 Laboratory studies have demonstrated that secondary organic aerosols (SOA) produced from diluted vehicle exhaust frequently
125 exceed the levels of primary organic aerosols (POA) in less than one day of atmospheric equivalent aging (Chirico et al., 2010;
126 Nordin et al., 2013; Platt et al., 2013; Gordon et al., 2014b; Liu et al., 2015). Oxidation flow reactors (OFRs) enable the
127 simulation of several days of atmospheric aging in a few minutes, with minimized wall effects compared to traditional smog
128 chamber experiments (Palm et al., 2016; Bruns et al., 2015). OFRs have been extensively employed to assess the SOA
129 formation potential of ambient air and emissions from diverse sources, including motor exhausts (Tkacik et al., 2014; Bruns
130 et al., 2015; Simonen et al., 2017; Watne et al., 2018; Liu et al., 2019b; Kuittinen et al., 2021; Zhou et al., 2021; Liao et al.,
131 2021a; Yao et al., 2022). In real-world traffic scenarios, the rapid response capabilities and convenient deployment of OFRs,
132 coupled with roadside point measurements, provide a robust method for evaluating emissions from a significant number of
133 vehicles. This approach effectively captures the considerable variability among individual vehicles within a fleet, offering a

134 comprehensive view of emissions under actual driving conditions (Watne et al., 2018; Zhou et al., 2021), although it may not
135 encompass as extensive a range of engine operations as setups that integrate OFRs with chassis dynamometer tests (Kuittinen
136 et al., 2021).

137

138 Primary emissions can also be oxidized to higher-volatility products through fragmentation reactions, potentially producing
139 carboxylic acids (Friedman et al., 2017). Engine exhaust is a recognized primary source of organic and inorganic acids in urban
140 environments (Kawamura et al., 1985; Kawamura and Kaplan, 1987; Kirchstetter et al., 1996; Wentzell et al., 2013; Friedman
141 et al., 2017). Monocarboxylic acids are produced by both diesel and spark-ignited engines (Zervas et al., 2001b; Crisp et al.,
142 2014; Zervas et al., 2001a; Kawamura et al., 1985). Recent studies have identified gaseous dicarboxylic acids in diesel
143 exhaust (Arnold et al., 2012), compounds likely linked to the nucleation and growth of particles (Zhang et al., 2004; Pirjola et
144 al., 2015). Additionally, inorganic acids such as nitric (HNO₃) and nitrous (HONO) acids, along with isocyanic acid (HNCO)—
145 implicated in serious health issues like atherosclerosis, cataracts, and rheumatoid arthritis through carbamylation reactions—
146 have been identified in both diesel and gasoline exhausts (Wang et al., 2007; Roberts et al., 2011; Wentzell et al., 2013; Brady
147 et al., 2014; Link et al., 2016; Li et al., 2021). However, the secondary production of organic acid from engine exhaust remains
148 poorly characterized; and it may significantly contribute to the overall organic acid budget and help explain discrepancies
149 between models and measurements (Paulot et al., 2011; Millet et al., 2015; Yuan et al., 2015). Furthermore, the impacts of
150 evolving fuel and engine technologies on emissions have not been comprehensively assessed. Recent advancements in
151 analytical techniques now enable simultaneous, high-resolution online measurements of both gas and particle phase acidic
152 species. This is facilitated by high-resolution time-of-flight chemical ionization mass spectrometry (HR-ToF-CIMS) using
153 acetate as the reagent ion, coupled with a filter inlet for gases and aerosols (FIGAERO) (Le Breton et al., 2019; Friedman et
154 al., 2017; Lopez-Hilfiker et al., 2014).

155

156 In this study, we present the findings from the photochemical aging of emissions from a modern on-road bus fleet operating
157 on diesel (DSL) and the latest generation of alternative fuels, including compressed natural gas (CNG), rapeseed methyl ester
158 (RME), and hydrotreated vegetable oil (HVO), using an oxidation flow reactor (Gothenburg Potential Aerosol Mass Reactor,
159 Go:PAM). We aim to compare the secondary production of PM from individual buses in real traffic with their primary PM
160 emissions, examining the impact of fuel type, engine technology, and photochemical age. Furthermore, both fresh and aged
161 emissions of gas and particle phases are characterized using HR-ToF-CIMS, providing a comprehensive understanding of the
162 emissions profile and their environmental implications.

163

164 In this study, we employed the OFR Gothenburg Potential Aerosol Mass Reactor (Go:PAM) along with roadside point
165 measurements to capture emissions from a diverse array of fuel types and engine technologies in in-use transit buses. We
166 present findings on the photochemical aging of emissions from a modern fleet operating on diesel (DSL) and the latest
167 generation of alternative fuels, including compressed natural gas (CNG), rapeseed methyl ester (RME), and hydrotreated

168 vegetable oil (HVO). Our study aims to compare the secondary production of PM from individual buses in real traffic scenarios
169 to their primary PM emissions, examining the impact of fuel type, engine technology, and photochemical age. Furthermore,
170 both fresh and aged emissions of gas and particle phases are characterized using HR-ToF-CIMS, providing a comprehensive
171 understanding of the emissions profile and their environmental implications.

172

173 **2. Methods**

174 **2.1 Emission measurements**

175 Roadside measurements were conducted at a designated urban bus stop, featuring a bus-only lane, in Gothenburg, Sweden,
176 (Supporting information (SI), Figure S1). The sampling occurred from March 2nd to 12th, 2016, with the average temperature
177 during this period recorded at approximately 3.9°C. Extractive sampling of individual bus plumes in real traffic was used to
178 characterize emissions, adhering to the method outlined by Hallquist et al. (2013). Air was continuously drawn through a cord-
179 reinforced flexible conductive hose to the instruments housed within a nearby container. Additional details of the experimental
180 conditions are available in our prior publication by Liu et al. (2019a). ~~Roadside measurements were conducted at a designated~~
181 ~~urban bus stop, featuring a bus-only lane, in Gothenburg, Sweden. (Supporting information (SI), Figure S1). Extractive~~
182 ~~sampling of individual bus plumes in real traffic was used to characterize emissions, adhering to the method outlined by~~
183 ~~Hallquist et al. (2013). More details of the experimental conditions are available in our prior publication by Liu et al. (2019a).~~

184 The primary focus of this study was to utilize the OFR Go:PAM and the HR-ToF-CIMS to explore the potential for secondary
185 pollutant formation and to conduct a detailed chemical characterization of both gas and particle phase compounds. An
186 experimental schematic of the roadside sampling is shown in Figure S2. Briefly, the emissions from passing bus plumes were
187 characterized as they accelerated from standstill at the bus stop. A camera was positioned at the roadside to capture bus plate
188 numbers, facilitating bus identification and enabling the collection of specific information on each bus, including fuel type,
189 engine technology, and exhaust after-treatment systems. The effective identification of emissions from individual buses was
190 achieved by employing CO₂ as a tracer, as delineated by Hak et al. (2009). The concentration of CO₂ was measured with a
191 non-dispersive infrared gas analyzer (LI-840A, time resolution 1 Hz). NO and NO_x were measured with two separate
192 chemiluminescent analyzers (Thermo Scientific™ Model 42i NO-NO₂-NO_x Analyzer). In addition, specific gaseous
193 compounds like CO, NO, and THC, were measured using a remote sensing device (AccuScan RSD 3000, Environmental
194 System Products Inc.). Particle emissions were characterized using a high time resolution engine exhaust particle sizer
195 spectrometer (EEPS, Model 3090 TSI Inc., time resolution 10 Hz) across a size range of 5.6-560 nm. Due to the lack of detailed
196 knowledge about the chemical composition of the emitted particles, particle mass calculations were based on the assumption
197 of spherical particles of unit density.

198

199 The HR-ToF-CIMS coupled with a FIGAERO was used to derive chemical information of both gas and particle phase species.
200 A detailed description of the configuration of the instrument can be found elsewhere (Aljawhary et al., 2013; Lopez-Hilfiker
201 et al., 2014; Le Breton et al., 2018; Le Breton et al., 2019). Acetate, employed as the reagent ion, was generated using an acetic
202 anhydride permeation source through a ^{210}Po ion source (^{210}Po inline ionizer, NRD inc, Static Solutions Limited). In the ion-
203 molecular reaction (IMR) chamber, the gaseous sampling flow interacted with the reagent ions, leading to the ionization of
204 target molecules. The dual inlets of the FIGAERO enable simultaneous gas phase sampling directly into the IMR and particle
205 sample collection on a PTFE filter for the duration of the plume via a separate inlet. The duration of the target plume for
206 particle collection was indicated by ~~particle number (PN)~~PN concentration measured by the EEPS. Once the PN concentration
207 reduced to undistinguishable at background levels, the filter was automatically positioned to allow the collected particles to be
208 evaporated into the IMR. The nitrogen flow over the filter was incrementally heated from room temperature to 200°C within
209 5 minutes and then maintained at this maximum temperature for 8 minutes, ensuring complete desorption of mass from the
210 filter, followed by analysis via HR-ToF-CIMS. Perfluoropentanoic acid (PFPA), a reliable high mass calibrant, was injected
211 into the CIMS inlet during the sampling period (Le Breton et al., 2019). Mass spectra were calibrated using known masses
212 (m/z), accurate within 4 ppm: O_2^- , CNO^- , $\text{C}_3\text{H}_5\text{O}_3^-$, $\text{C}_2\text{F}_3\text{O}_3^-$, $\text{C}_5\text{F}_9\text{O}_2^-$, $\text{C}_{10}\text{F}_{18}\text{O}_4^-$, covering a range of 32-526 m/z (more details
213 can be found in SI). The data were acquired at 1 s time resolution. To estimate absolute EFs, a conversion of the CIMS signal
214 to concentration using a sensitivity factor is necessary. Based on the method of Lopez-Hilfiker et al. (2015), the maximum
215 sensitivity was determined to be 20 Hz ppt⁻¹, which falls within previously reported ranges (Mohr et al., 2017). Using this
216 maximum sensitivity provides a lower-limit estimate of EFs for all oxygenated volatile organic compounds (Zhou et al., 2021).
217 The assumption on sensitivity did not affect the comparative analysis of EFs with respect to different fuel types.

218

219 The EFs of constituents per kilogram of fuel burnt were calculated by relating the concentration change of a specific compound
220 in the diluted exhaust plume to the change in CO_2 concentration. CO_2 served as a tracer for exhaust gas dilution, relative to
221 background concentration (Janhäll and Hallquist, 2005; Hak et al., 2009; Hallquist et al., 2013; Watne et al., 2018).
222 ~~Assumptions were made for complete combustion and carbon contents of 86.1, 77.3, 70.5, and 69.2% for DSL, RME, HVO,~~
223 ~~and CNG, respectively, were assumed (Edwards et al., 2004). Further methodological details are elaborated in Liu et al.~~
224 ~~(2019a). A more comprehensive description of the EF calculations is provided in the Supporting Information. In the~~
225 ~~calculations, complete combustion and carbon contents of 86.1, 77.3, 70.5, and 69.2% for DSL, RME, HVO, and CNG,~~
226 ~~respectively, were assumed (Edwards et al., 2004). Further methodological details are elaborated in Liu et al. (2019a).~~

227

228 **2.2 Oxidation flow reactor setup**

229 The OFR Go:PAM was utilized for photochemical aging of emissions from individual buses to investigate the potential for
230 secondary pollutant formation. The comprehensive description and operational protocols of the Go:PAM have been detailed
231 previously (Watne et al., 2018; Zhou et al., 2021). Briefly, the Go:PAM is a 6.1 L continuous-flow quartz glass flow reactor
232 with input flows such that the median residence time is approximately 37s. The reactor is equipped with two Philips TUV 30

233 W fluorescent lamps ($\lambda = 254$ nm) and enclosed by reflective and polished aluminium mirrors to ensure a homogeneous photon
234 field. The UV lamps generate OH radicals through the photolysis of O_3 in the presence of water vapor. The relative humidity
235 (RH) within the reactor was around 60 - 80%. The O_3 concentration inside the Go:PAM was measured using an ozone monitor
236 (2B technology, model 205 dual beam ozone monitor) at around 880 ppb prior to the introduction of vehicle exhaust. Particle
237 wall losses in the Go:PAM were corrected using size-dependent transmission efficiency (Watne et al., 2018). The OH exposure
238 (OH_{exp}) inside the Go:PAM was calibrated offline using sulfur dioxide (SO_2), following methodologies established in previous
239 studies (Lambe et al., 2011; Kang et al., 2007), with additional details provided in the SI. During on-road measurements, the
240 OH_{exp} may be significantly influenced by the OH reactivity (i.e., CO and HC) and titration of O_3 by NO in the plumes, which
241 varied between vehicles. Thus, the OH reactivity was estimated for each bus passage using the maximum NO_x , CO and HC
242 concentrations in the Go:PAM, along with corresponding water and ozone levels (Watne et al., 2018; Zhou et al., 2021).
243 Employing the maximum concentrations of these OH- or O_3 -consuming species represents a minimum estimate of OH_{exp} in
244 our calculations. The flow-design incorporated in the Go:PAM enables investigation of transient phenomena, such as passing
245 plumes. It also works at relatively low ozone concentrations (less than 1 ppm), limiting reactions of other potential oxidants
246 such as O_3 , NO_3 , or O^1D (Zhou et al., 2021).

247

248 3. Results and discussion

249 3.1 Fresh and aged PM emissions from buses

250 The aged PM emissions ($EF_{PM:aged}$) of 133 plumes from a diverse set of buses, including 16 ~~diesel (DSL)~~DSL, 11 ~~compressed~~
251 ~~natural gas (CNG)~~CNG, 20 ~~rapeseed methyl ester (RME)~~RME, 20 ~~hydrotreated vegetable oil (HVO)~~HVO and 9 hybrid-
252 electric HVO (HVO_{HEV}) buses, were investigated using Go:PAM. The corresponding average fresh PM emissions ($EF_{PM:Fresh}$)
253 for these 76 buses were measured during several sequential days (Figure S2). These buses were a subset of the 234 buses
254 described in our previous study (Liu et al., 2019a), and represent data corresponding to available Go:PAM measurements. A
255 comprehensive discussion on the full data set for fresh condition is available in Liu et al. (2019a). Figure 1 shows the average
256 $EF_{PM:Fresh}$ and $EF_{PM:aged}$ with respect to fuel type. Among the buses, Euro V DSL models had the highest median $EF_{PM:Fresh}$,
257 $MdEF_{PM:Fresh}$ (represented by the horizontal yellow lines), of 208 mg kg-fuel⁻¹, followed by HVO_{HEV} , RME and HVO buses with
258 $MdEF_{PM:Fresh}$ of 109, 74 and 62 mg kg-fuel⁻¹ respectively. CNG buses and HVO_{HEV} buses equipped with a DPF under Euro VI
259 standards exhibited the lowest $MdEF_{PM:Fresh}$, with over half of these buses exhibiting $EF_{PM:Fresh}$ below the detection limit (<4.3
260 mg kg-fuel⁻¹). Except for HVO_{HEV} buses with a DPF, which was limited to a small tested number, all other bus types in this
261 subset had $MdEF_{PM:Fresh}$ comparable to those of the full data set in Liu et al. (2019a), within $\pm 30\%$ and following the same rank
262 order. The average EFs of fresh and aged particle emissions and general gaseous pollutants for individual buses are given in
263 Table 1.

264

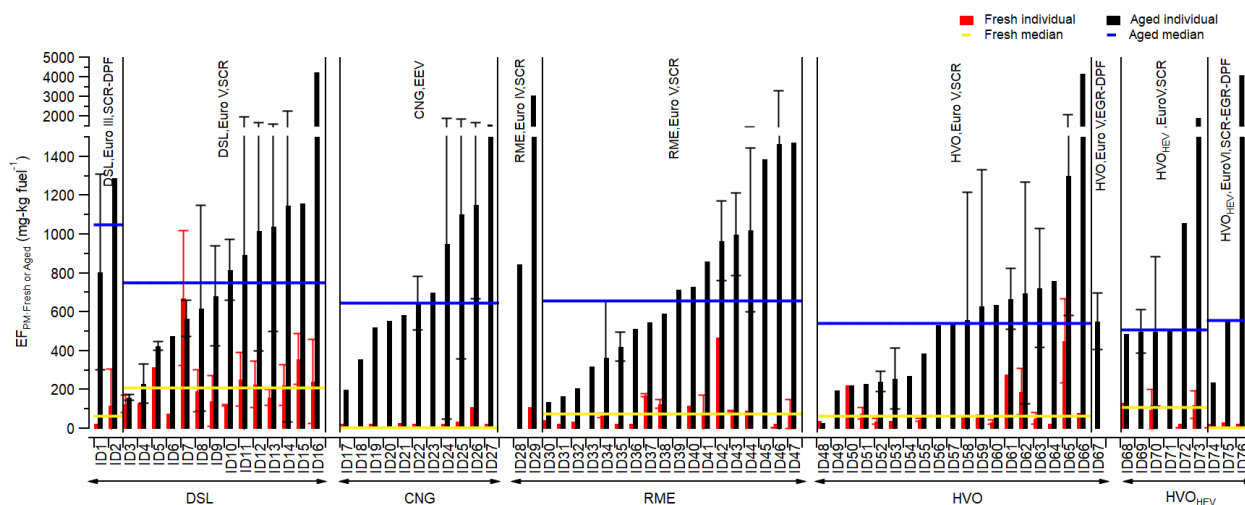
265 After photooxidation in Go:PAM, particle mass increased markedly, with half of the individual buses showing average
266 $EF_{PM:aged}$ more than eight times their average $EF_{PM:Fresh}$. For all Euro V/ EEV buses, the median $EF_{PM:aged}$, $MdEF_{PM:aged}$
267 (represented by the horizontal blue lines), was highest for DSL buses of $749 \text{ mg kg-fuel}^{-1}$ followed by a descending order of
268 RME (655) > CNG (645) > HVO (543) > HVO_{HEV} (509). Despite low $EF_{PM:Fresh}$, CNG buses produced substantial secondary
269 particle mass. The DPF, proven effective in earlier studies (Martinet et al., 2017; Preble et al., 2015; May et al., 2014),
270 efficiently reduced primary particle emissions from DSL Euro III and HVO_{HEV} Euro VI buses. However, these bus types, even
271 with DPFs, exhibited higher $EF_{PM:aged}$ than those using the same fuels but without DPFs (Euro V), albeit the number of tested
272 buses with DPFs was limited. The variance in median $EF_{PM:aged}$ among different fuel types was less pronounced compared to
273 $EF_{PM:Fresh}$, suggesting the presence of significant non-fuel-dependent precursor sources, such as lubrication oils and/or fuel
274 additives (Watne et al., 2018; Le Breton et al., 2019).

275
276 ~~Figure 2 shows the bus average $EF_{PM:Fresh}$ vs the corresponding $EF_{PM:aged}$ for individual bus passages, where the average~~
277 ~~$EF_{PM:aged}$ for each bus is indicated by a solid horizontal line. This analysis focuses on Euro V/EEV buses to ensure high number~~
278 ~~of buses in the comparison, while buses from other Euro classes were not included due to their limited numbers. $EF_{PM:aged}$~~
279 ~~exhibited notable variation between passages of the same bus, likely attributable to emission variability between passages and~~
280 ~~differing dilution levels for plumes prior to sampling into the Go:PAM. The median ratio of $EF_{PM:aged}$ to $EF_{PM:Fresh}$ was highest~~
281 ~~for CNG buses (84), followed by RME (10.8), HVO_{HEV} (10.5), HVO (6.7) and DSL(4.0) buses. Buses equipped with DPFs,~~
282 ~~including DSL Euro III and HVO_{HEV} Euro VI (not included in Figure 2), exhibited a median ratio exceeding 50. In Figure 2b,~~
283 ~~$EF_{PM:Fresh}$ and $EF_{PM:aged}$ are presented as a function of the dilution level, indicated by the integrated CO_2 area. Some buses had~~
284 ~~primary emissions too dilute for detection (markers located to the left in Figure 2b) but still showed non negligible $EF_{PM:aged}$~~
285 ~~upon oxidation. To examine the effects of simulated atmospheric oxidation in the Go:PAM, an estimated minimum OH_{exp} was~~
286 ~~calculated for each plume by incorporating the OH reactivities of CO and HC and the titration of O_3 with NO, following~~
287 ~~methodologies from Watne et al. (2018) and Zhou et al. (2021). For all plumes, OH_{exp} varied between 1.1×10^9 to 4.6×10^{11}~~
288 ~~molecules $cm^{-3} \cdot s$. The $EF_{PM:aged}$ for some buses, for example, the DSL and HVO located to the right in Figure 2c, increased~~
289 ~~with increasing OH_{exp} . However, due to potential large differences in emissions together with dilution effects across different~~
290 ~~passages, the OH_{exp} dependent $EF_{PM:aged}$ for other buses was less pronounced.~~

291
292 Figure 2 shows the bus average $EF_{PM:Fresh}$ vs the corresponding $EF_{PM:aged}$ for individual bus passages, where the average
293 $EF_{PM:aged}$ for each bus is indicated by a solid horizontal line. This analysis focuses on Euro V/EEV buses to ensure a sufficient
294 number of buses in the comparison, while buses from other Euro classes were not included due to their limited numbers. The
295 median ratio of $EF_{PM:aged}$ to $EF_{PM:Fresh}$ was highest for CNG buses (84), followed by RME (10.8), HVO_{HEV} (10.5), HVO (6.7)
296 and DSL(4.0) buses. Buses equipped with DPFs, such as DSL Euro III and HVO_{HEV} Euro VI (not included in Figure 2),
297 exhibited a median ratio exceeding 50. $EF_{PM:aged}$ exhibited notable variation between passages of the same bus, likely
298 attributable to emission variability between passages and different dilution levels for plumes prior to sampling into the

299 Go:PAM. This is illustrated in Figure 2b, where $EF_{PM:Fresh}$ and $EF_{PM:aged}$ are presented as a function of the dilution level,
 300 indicated by the integrated CO_2 area. Generally, a higher integrated CO_2 area suggests a more concentrated plume, leading to
 301 increased external OH and O_3 reactivity, which in turn reduces the concentration of OH radicals available in the Go:PAM for
 302 precursor oxidation (Emanuelsson et al., 2013; Watne et al., 2018). Some buses displayed primary emissions too dilute for
 303 detection (markers located to the left in Figure 2b) but still exhibited non-negligible $EF_{PM:aged}$ after oxidation. To further
 304 examine the effects of simulated atmospheric oxidation in the Go:PAM, an estimated minimum OH_{exp} was calculated for each
 305 plume by incorporating the OH reactivities of CO and HC and the titration of O_3 with NO, following methodologies from
 306 Watne et al. (2018) and Zhou et al. (2021). For all plumes, OH_{exp} varied between 1.1×10^9 to 4.6×10^{11} molecules $cm^{-3} s$. The
 307 $EF_{PM:aged}$ for some buses, for example, the DSL and HVO located to the right in Figure 2c, increased with increasing OH_{exp} .
 308 However, due to potential large differences in the chemical composition of emissions across different passages of the same
 309 bus, where some species are more prone to forming secondary particle mass even at lower OH_{exp} , the OH_{exp} dependent $EF_{PM:aged}$
 310 for other buses was less pronounced.

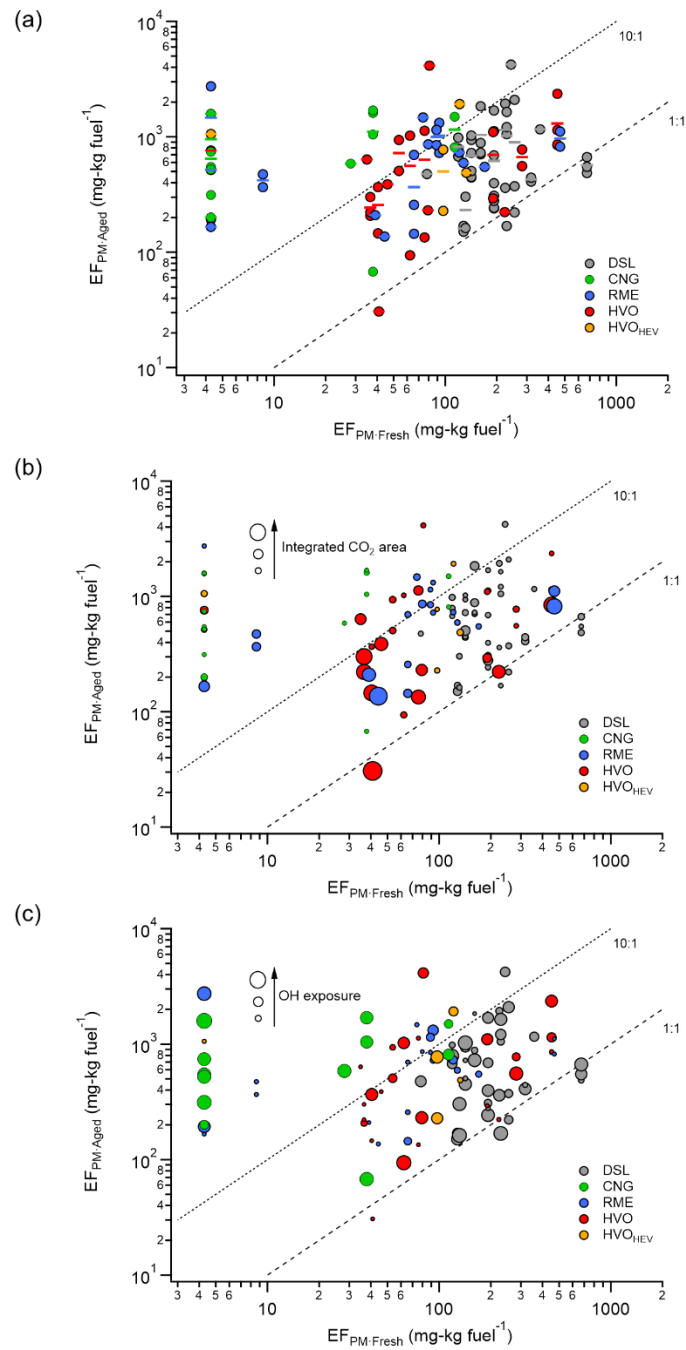
311



312

313 Figure 1. $EF_{PM:Fresh}$ (red bar) and $EF_{PM:aged}$ (black bar) with respect to fuel class: DSL (diesel, ID₁-ID₁₆), CNG (compressed
 314 natural gas, ID₁₇-ID₂₇), RME (rapeseed methyl ester, ID₂₈-ID₄₇), HVO (rapeseed methyl ester, ID₄₈-ID₆₇) and HVO_{HEV} (hybrid-
 315 electric HVO, ID₆₈-ID₇₆) buses. Median values for $EF_{PM:Fresh}$ ($^{Md}EF_{PM:Fresh}$) and $EF_{PM:aged}$ ($^{Md}EF_{PM:aged}$) are indicated by
 316 horizontal yellow and blue lines, respectively. The information on engine technology and exhaust after-treatment systems is
 317 also shown. Given errors represent the standard deviation (1σ).

318



319

320

321 Figure 2. $EF_{PM:aged}$ vs average $EF_{PM:Fresh}$ for all the studied bus passages (Euro V) with respect to fuel type (a) and as a function
 322 of integrated CO₂ area (b) and OH exposure (OH_{exp}) (c). The dashed lines denote the 10:1 and 1:1 $EF_{PM:aged}$: $EF_{PM:Fresh}$ ratios,
 323 and the solid lines in (a) represent bus averages. One may note that the buses with $EF_{PM:Fresh}$ values below detection limit were

324 set to 4.3 mg kg-fuel⁻¹. Abbreviations: DSL (diesel), CNG (compressed natural gas), RME (rapeseed methyl ester), HVO
 325 (hydrotreated vegetable oil), HVO_{HEV} (hybrid-electric HVO).

326

327 Table 1. Average particle and gaseous EFs of individual buses for fresh emissions and average EF_{PM} for aged emissions^a.

Bus ID	Fuel ^c	Euro standard	Exhaust after-treatment system ^d	EF _{PM:Fresh} (mg kg ⁻¹ _{fuel})	EF _{PN:Fresh} (10 ¹⁴ # kg ⁻¹ _{fuel})	EF _{CO} (g kg ⁻¹ _{fuel})	EF _{THC} (g kg ⁻¹ _{fuel})	EF _{NOx} (g kg ⁻¹ _{fuel})	EF _{PM:Aged} (mg kg ⁻¹ _{fuel})
1	DSL	III	SCR, DPF	4.3	0.41	3.9±11	1.5±2.9	10±3.2	810±510
2	DSL	III	SCR, DPF	120±190	34±61	2.7±7	1.7±3.7	11±5	1300
3	DSL	V	SCR	130±45	3.3±1.3	17±18	0.35±1.3	3.9±3.7	160±13
4	DSL	V	SCR	130	3.6	20±22	1.5±3.6	4.7±7.2	230±100
5	DSL	V	SCR	320	5.9	20±28	2±3.5	9.7±7	430±23
6	DSL	V	SCR	78	1.6	20±21	2.7±5.6	13±12	480
7	DSL	V	SCR	670±350	10±6.8	42±44	2.3±3.7	6.8±5	570±92
8	DSL	V	SCR	190±110	6.5±3	14±21	0.75±1.7	12±5.1	620±530
9	DSL	V	SCR	140±130	4.3±2.6	9.8±14	1±1.5	15±13	680±260
10	DSL	V	SCR	120±4.7	3.2±0.66	16±18	2.5±4.7	12±6.9	820±160
11	DSL	V	SCR	250±140	4.7±2.7	16±23	0.8±1.4	12±8.9	900±1000
12	DSL	V	SCR	230±120	5.1±1.5	16±26	2.6±4.6	12±9.9	1000±620
13	DSL	V	SCR	160±41	3.5±0.97	27±27	1.4±2.7	17±9.8	1000±540
14	DSL	V	SCR	220±110	5.2±1.3	12±17	2.6±4.1	11±7.4	1100±1100
15	DSL	V	SCR	360±130	6.8±4.2	21±25	1.2±3.3	5.7±4.4	1200
16	DSL	V	SCR	240±220	22±11	5.5±7.5	0.74±1.6	6.8±5.6	4200
17	CNG	EEV	-	4.3±0	0.41±0	n.a.	n.a.	4.8±1.7	200
18	CNG	EEV	-	n.a.	n.a.	n.a.	n.a.	11±4.9	360
19	CNG	EEV	-	4.3±0	0.41±0	n.a.	n.a.	4±3.8	520
20	CNG	EEV	-	n.a.	n.a.	n.a.	n.a.	15±17	560
21	CNG	EEV	-	28	1.3	n.a.	n.a.	2.2±0.93	590
22	CNG	EEV	-	4.3	0.41	n.a.	n.a.	1.8±1	650±140
23	CNG	EEV	-	n.a.	n.a.	n.a.	n.a.	3.2±0.53	700
24	CNG	EEV	-	4.3	0.41	n.a.	n.a.	6.9±1.4	950±900
25	CNG	EEV	-	38	11	n.a.	n.a.	7.3±5.3	1100±750
26	CNG	EEV	-	110	200	n.a.	n.a.	8.2±4.2	1200±480
27	CNG	EEV	-	4.3±0	0.41±0	n.a.	n.a.	6±1.8	1600
28	RME	IV	SCR	n.a.	n.a.	10±8.7	3.1±3	46±20	850
29	RME	IV	SCR	110	4.1	4.2±8.4	0.19±0.38	7.2±6.8	3000
30	RME	V	SCR	44	2.2	12±14	2.2±3.6	32±32	140
31	RME	V	SCR	4.3	0.41	7.4±7.1	0.075±0.17	13±5.1	170
32	RME	V	SCR	39	6.2	5.2±4.8	0.87±1.1	18±5.4	210
33	RME	V	SCR	n.a.	n.a.	0.24±0.54	0.24±0.39	10±3.3	320
34	RME	V	SCR	66±11	2.4±1	7±7.2	1.8±2.7	23±13	370±290
35	RME	V	SCR	8.6	0.96	4.9±3.6	0.59±0.73	20±5.1	420±75
36	RME	V	SCR	4.3	0.41	22±23	1.8±2	25±16	520
37	RME	V	SCR	170±7.7	6.4±1	34±35	0.016±0.043	19±10	550
38	RME	V	SCR	130±24	11±14	17±20	2±4	16±15	590
39	RME	V	SCR	n.a.	n.a.	1.2	0.64	21	720
40	RME	V	SCR	120	5.3	12±9.4	1.8±2.6	18±8.2	730
41	RME	V	SCR	80±95	4.2±2.9	8.8±17	0.72±0.87	25±5.7	860
42	RME	V	SCR	470	5.8	4.5±5.1	0.23±0.38	18±7.8	970±210
43	RME	V	SCR	89±2.3	2.6±0.16	5.4±9.4	0.68±1.9	28±17	1000±210
44	RME	V	SCR	92	1.6	14±19	1.8±3	23±17	1000±420
45	RME	V	SCR	n.a.	n.a.	37±26	5.8±3.6	14±6.3	1400
46	RME	V	SCR	4.3±0	0.41±0	9.6±14	0.89±1.4	28±8.4	1500±1800
47	RME	V	SCR	74±75	12±6	6.1±6.3	1.1±1.4	18±5.2	1500
48	HVO	V	SCR	41	1.5	8.4±2	0.14±0.31	10±0.4	31
49	HVO	V	SCR	n.a.	n.a.	5.8±8	0.7±0.62	13±10	200
50	HVO	V	SCR	220	6.6	8.3±9.1	0.91±0.97	13±8.6	220
51	HVO	V	SCR	79±31	2.6±0.74	7.8±5.8	0.41±0.59	12±8.2	230

52	HVO	V	SCR	37±13	1.9±0.65	4.8±5.5	0.64±0.82	20±3	240±51
53	HVO	V	SCR	40	2.5	2.1±3.4	0.0083±0.019	16±4.3	260±160
54	HVO	V	SCR	n.a.	n.a.	2.1±3	0.55±0.77	22	270
55	HVO	V	SCR	46±6.6	2.6±0.52	6.2±4.1	0.79±0.55	12±8.2	390
56	HVO	V	SCR	n.a.	n.a.	11±10	0.74±0.84	5.7	530
57	HVO	V	SCR	n.a.	n.a.	14±17	0.79±1.2	11±2.6	540
58	HVO	V	SCR	62	4.1	6.8±6.7	0.22±0.31	11±6.3	560±660
59	HVO	V	SCR	76	5.3	2.3±2	0.24±0.47	19±3.4	630±700
60	HVO	V	SCR	35±11	1.5±0.19	3.3±5	0.45±0.86	9.2±9	640
61	HVO	V	SCR	280	14	9.9±16	0.55±0.73	11±3.6	670±160
62	HVO	V	SCR	190±120	68±86	1.1±1.9	0.3±0.49	9.3±4.9	700±570
63	HVO	V	SCR	54±30	4.6±2.2	3.5±4.6	0.49±0.48	14±3.5	720±310
64	HVO	V	SCR	4.3	0.41	2.2±3.8	0.33±0.73	12±4.8	760
65	HVO	V	SCR	450±220	18±18	1.4±1.6	0.28±0.37	12±2.6	1300±720
66	HVO	V	SCR	81	11	0.88±0.93	0.28±0.25	13±6.5	4100
67	HVO	V	EGR, DPF	n.a.	n.a.	4.6±5.9	0.64±1.2	11±8.1	550±150
68	HVO _{HEV}	V	SCR	130	52	12±19	0.97±1.4	20±15	490
69	HVO _{HEV}	V	SCR	n.a.	n.a.	4.1±8.4	0.5±1.3	18±3.3	500±110
70	HVO _{HEV}	V	SCR	97±100	25±18	3.8±6.8	1.1±1.8	17±5.7	500±390
71	HVO _{HEV}	V	SCR	n.a.	n.a.	7.6±9.9	2.9±2.4	12±2.1	520
72	HVO _{HEV}	V	SCR	4.3±0	0.41±0	3.7±5.8	1±2.4	20±10	1100
73	HVO _{HEV}	V	SCR	120±72	8.9±2.9	1.2±1.7	0.18±0.26	17±7	1900
74	HVO _{HEV}	VI	SCR,EGR,DPF	4.3±0	0.41±0	4.7±11	2.2±4.7	7.2±8.5	240
75	HVO _{HEV}	VI	SCR,EGR,DPF	33	29	1.2±2.4	0.22±0.49	6.7±3.3	550
76	HVO _{HEV}	VI	SCR,EGR,DPF	4.3	0.41	10±9.2	1.5±2.3	8.8±8.7	4100

328

329

^aGiven errors represent the standard deviation (1σ).

330

^bn.a., abbreviation for not available.

331

^cDSL, CNG, RME, HVO and HVO_{HEV}, abbreviations for diesel, compressed natural gas, rapeseed methyl ester, hydrotreated vegetable oil, and hybrid-electric hydrotreated vegetable oil.

332

333

^dSCR, DPF and EGR, abbreviations for selective catalytic reduction, diesel particulate filter and exhaust gas recirculation systems.

334

335

336

337 The secondary particle mass formed (ΔPM) was calculated as the difference between $EF_{PM,aged}$ for a plume and the average

338 $EF_{PM:Fresh}$ for the corresponding individual bus. ~~Figure 3 shows the ΔPM as a function of OH_{exp} for all bus types during the~~

339 ~~Go-PAM measurements. Figure 3 illustrates ΔPM as a function of OH_{exp} for the bus fleet in this study, which includes 40%~~

340 ~~DSL, 12.2% CNG, 20% RME, 20.8% HVO, and 7% HVO_{HEV}. The results were grouped based on OH_{exp} , spanning a range~~

341 ~~from 1.1×10^9 to 4.6×10^{11} molecules cm^{-3} s.~~ The results in this study are compared with those reported from a tunnel

342 study (Tkacik et al., 2014), an urban roadside study of a mixed fleet in Hong Kong (Liu et al., 2019b), a depot study on rather

343 modern types of city buses (Watne et al., 2018) and roadside measurements of a heavy-duty truck fleet in Gothenburg (Zhou

344 et al., 2021). Laboratory OFR and chamber studies of middle-duty and heavy-duty diesel vehicles (Deng et al., 2017), diesel

345 passenger cars (Chirico et al., 2010), a diesel engine (Jathar et al., 2017a), and gasoline vehicles (Gordon et al., 2014a; Platt

346 et al., 2013) were also included for comparison.

347

348 The ΔPM from vehicle emissions is influenced by factors such as vehicle and fuel types, driving modes, and OH_{exp} during

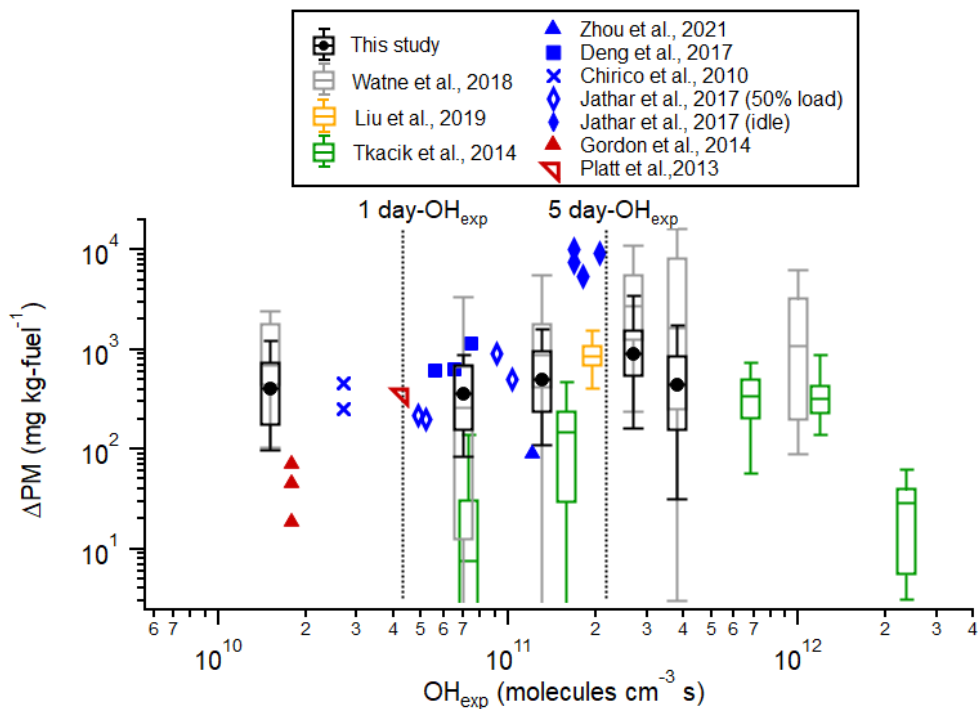
349 experiments (Gentner et al., 2017). Considering the variability of OH reactivity among vehicles and the consequently wide

350 range of OH_{exp} , this study, along with Watne et al. (2018), categorizes ΔPM trend into OH_{exp} bins. The median ΔPM was

351 approximately $400 \text{ mg kg-fuel}^{-1}$ at $OH_{exp} < 4.3 \times 10^{10}$ molecules cm^{-3} s (corresponding to 1 OH day, assuming an OH

352 concentration of 1×10^6 molecules cm^{-3} for 12 h per day) and was 364-495 mg kg-fuel^{-1} at 1-5 OH days, reaching a maximum
353 of around 920 mg kg-fuel^{-1} at approximately 5-6 OH days for the bus fleet in this study, ~~comprising 40% DSL, 12.2% CNG,~~
354 ~~20% RME, 20.8% HVO, and 7% HVO_{HEV} buses.~~ This peak value of ΔPM was lower than the approximately 3000 mg kg-fuel^{-1}
355 at ~5-6 OH days observed in the depot measurements by Watne et al. (2018), a difference potentially due to variations in
356 engine technology and fuel types used in the bus fleets. Notably, HVO was not used in the depot study, while some buses
357 switched from RME to HVO prior to this study. The ΔPM peaked and then decreased at higher OH_{exp} , likely due to the
358 transition from functionalization-dominated reactions and condensation at lower OH_{exp} to fragmentation reactions and
359 evaporation dominance at higher OH_{exp} (Tkacik et al., 2014; Ortega et al., 2016). The ΔPM in this study was comparable to
360 855 mg kg-fuel^{-1} for a mixed fleet consisting of 44.1% gasoline, 41.3% diesel, and 14.6% LPG vehicles measured at an urban
361 roadside in Hong Kong (Liu et al., 2019b), ~~and was slightly higher than that of a Euro VI dominated (more than 70%) heavy-~~
362 ~~duty truck fleet measured at an urban roadside site in Gothenburg (Zhou et al., 2021). It was slightly higher than the ΔPM~~
363 ~~measured from a Euro VI dominated (more than 70%) heavy-duty truck fleet at an urban roadside in Gothenburg (Zhou et al.,~~
364 ~~2021), and from a fleet with over 80% light-duty gasoline vehicles in a Pittsburgh tunnel study (Tkacik et al., 2014).~~
365 Additionally, the ΔPM in this study was consistent with that for middle-duty and heavy-duty diesel vehicles (Deng et al.,
366 2017), diesel passenger cars (Chirico et al., 2010), and a diesel (or biodiesel)-fuelled engine under 50% load condition (Jathar
367 et al., 2017a) (around 190-1133 mg kg-fuel^{-1}). However, the diesel (or biodiesel)-fuelled engine under idle conditions can
368 produce significantly higher ΔPM (more than 5000 mg kg-fuel^{-1}), likely because engines at idle loads are less efficient at
369 burning fuel, leading to higher emissions of unburnt gaseous combustion products (as precursors of secondary PM) (Nordin et
370 al., 2013; Saliba et al., 2017; Jathar et al., 2017a). In contrast, experiments conducted for gasoline vehicles at relatively low
371 photochemical ages (< 1 OH day) typically produced ΔPM lower than 70 mg kg-fuel^{-1} (Gordon et al., 2014a), except for a
372 Euro 5 gasoline vehicle (340 mg kg-fuel^{-1}) operated with a New European Driving Cycle (Platt et al., 2013).

373



374

375

376 Figure 3. Secondary particle mass formed (ΔPM), calculated as $\text{EF}_{\text{PM:aged}}$ subtracted by the average $\text{EF}_{\text{PM:Fresh}}$, vs modeled OH
 377 exposure (OH_{exp}) for the bus fleet in this study and comparison with those reported for a tunnel study (Tkacik et al., 2014), a
 378 depot study (Watne et al., 2018), roadside measurements (Liu et al., 2019b; Zhou et al., 2021), middle-duty and heavy-duty
 379 diesel vehicles (Deng et al., 2017), diesel passenger cars (Chirico et al., 2010), a diesel engine (Jathar et al., 2017a), and
 380 gasoline vehicles (Gordon et al., 2014a; Platt et al., 2013). Dashed lines indicate 1- and 5-day OH_{exp} assuming an OH
 381 concentration of 1×10^6 molecules cm^{-3} 12 h per day (Watne et al., 2018). Note that ΔPM in this study, alongside those by
 382 Watne et al. (2018), Zhou et al. (2021) and Liu et al. (2019b), includes both secondary organic and inorganic aerosol, while
 383 ΔPM in research by Deng et al. (2017), Chirico et al. (2010), Jathar et al. (2017a), Gordon et al. (2014a), Platt et al. (2013)
 384 and Tkacik et al. (2014) pertains only to secondary organic aerosol mass.

385

386

387

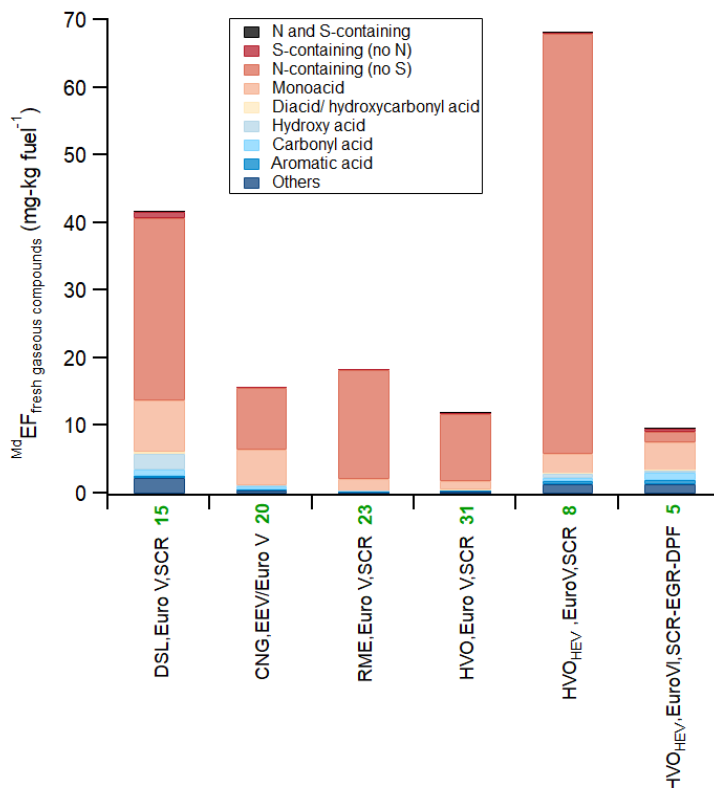
388 3.2 Chemical characterization using CIMS

389 3.2.1 Fresh gaseous emissions

390 Figure 4 presents the median emission factors ($^{\text{M}}\text{dEFs}$) of acetate-CIMS measured fresh gaseous emissions with respect to fuel
 391 type. The identities of the organic compounds detected by HR-ToF-CIMS are assigned based on knowledge of sensitivities of
 392 the ionization scheme and the expected compounds emitted from the buses. Plausible compounds are assigned from the

393 formulae, with a caveat that other isomers might contribute to the signal. These compounds were classified into nine families
394 based on their molecular characteristics as outlined by Liu et al. (2017), with additional details provided in the SI. Among all
395 Euro V/EEV buses, hybrid-electric HVO (HVO_{HEV}) buses exhibited the highest ^{Md}EF of CIMS measured fresh gaseous
396 emissions (68 mg kg-fuel⁻¹), followed by DSL (42 mg kg-fuel⁻¹), RME (18 mg kg-fuel⁻¹), and CNG (16 mg kg-fuel⁻¹), while
397 HVO had the lowest ^{Md}EF of 12 mg kg-fuel⁻¹. Nitrogen (N) -containing compounds (no sulfur) and monoacid families
398 predominantly composed these fresh gaseous emissions. Compared to Euro V HVO_{HEV} buses, HVO_{HEV} buses equipped with
399 exhaust gas recirculation (EGR) and DPF systems (Euro VI) demonstrated a significant reduction in ^{Md}EF (10 mg kg-fuel⁻¹),
400 primarily due to decreased emissions of N-containing compounds, although the ^{Md}EF of other compound families were higher.
401 In contrast, Zhou et al. (2021) reported significant reductions in both carboxylic acids and carbonyl compounds (by 94% on
402 average), and acidic nitrogen-containing organic and inorganic species (79%) when transitioning from Euro V to Euro VI
403 heavy-duty trucks. However, details on the types of exhaust after-treatment systems used in the trucks from such study are not
404 specified. Moreover, this study utilized acetate as a different reagent ion for CIMS compared to the iodide used by Zhou et al.
405 (2021). Table 2 lists the top 10 ^{Md}EFs of fresh gaseous compounds, contributing over 88% of total fresh gaseous emissions
406 measured by CIMS for most bus types, except for Euro VI HVO_{HEV} (61%). The fresh gaseous emissions from all types of Euro
407 V/EEV buses were primarily composed of nitrous acid (HONO) and nitric acid (HNO₃), with HONO being the most significant
408 acidic emission. The ^{Md}EFs of HONO and HNO₃ generally align with values reported in the literature, ranging from
409 approximately 7-250 mg kg-fuel⁻¹ for HONO (Kurtenbach et al., 2001; Wentzell et al., 2013; Liao et al., 2020; Nakashima and
410 Kondo, 2022) and around 4-14 mg kg-fuel⁻¹ for HNO₃ (Wentzell et al., 2013). Acetic acid (C₂H₄O₂), formic acid (CH₂O₂), and
411 isocyanic acid (HNCO) also exhibited relatively high ^{Md}EFs. The ^{Md}EFs of formic acid for all Euro V/EEV bus types (0.02-
412 1.97 mg kg-fuel⁻¹) were consistent with those from a light-duty gasoline fleet (0.57–0.94 mg kg-fuel⁻¹) reported by Crisp et al.
413 (2014). The ^{Md}EFs of acetic acid ranged from 1.23 to 4.84 mg kg-fuel⁻¹, falling between values for gasoline vehicles (0.78 mg
414 kg-fuel⁻¹) and diesel buses (approximately 12-23 mg kg-fuel⁻¹) (Li et al., 2021). Isocyanic acid, likely an intermediate product
415 of the thermal degradation of urea in SCR systems without sufficient hydrolysis (Bernhard et al., 2012), was detected in
416 emissions from all bus types, with ^{Md}EFs of 0.08-14.74 mg kg-fuel⁻¹. These values are slightly lower than those from a non-
417 road diesel engine (31-56 mg kg-fuel⁻¹) reported by Jathar et al. (2017b), but align well with SCR-equipped diesel vehicles
418 tested by Suarez-Bertoa and Astorga (2016) (1.3-9.7 mg kg-fuel⁻¹) and a diesel engine with a diesel oxidation catalyst
419 (DOC) (Wentzell et al., 2013) (0.21-3.96 mg kg-fuel⁻¹). Among all Euro V/EEV buses, HVO_{HEV} buses showed the highest
420 emissions of HNCO, potentially attributed to cold engine conditions since the combustion engine does not operate
421 continuously. Notably, emissions of HNCO were significantly lowered and neither HONO nor HNO₃ were identified among
422 the top 10 ^{Md}EFs for HVO_{HEV} buses equipped with EGR and DPF systems (Euro VI), suggesting that newer engine technologies
423 incorporating EGR and DPF systems likely effective in reducing emissions of NO_x (Table 1) as well as HNCO, HONO and
424 HNO₃. CH₄SO₃, potentially identified as methanesulfonic acid, was detected in the emissions from DSL and RME buses.
425 Previous studies, such as those by Corrêa and Arbilla (2008), have shown that mercaptans, emitted from diesel and biodiesel
426 exhausts, can transform under high NO_x conditions into products including methanesulfonic acid. The presence of sulfur-

427 containing organic compounds in diesel fuel and lubricants, and their potential transformation upon combustion into various
 428 sulfuric derivatives, alongside the catalytic activity of engine converters, could also contribute to such findings. However, the
 429 detailed formation pathway of CH₄SO₃ in our study remains unknown.
 430
 431



432
 433 Figure 4. MdEFs of CIMS measured fresh gaseous emissions with respect to fuel class: DSL (diesel, 15), CNG (compressed
 434 natural gas, 20), RME (rapeseed methyl ester, 23), HVO (rapeseed methyl ester, 31) and HVO_{HEV} (hybrid-electric HVO, 13)
 435 buses. The number in bold green represents the number of buses examined.

436

437

438 Table 2. Summary of top 10 MdEFs of fresh gaseous compounds measured using HR-ToF-CIMS of DSL, CNG, RME, HVO
 439 and HVO_{HEV} buses^a (color coded by different families shown in Figure 4).

DSL, Euro V, SCR		CNG, EEV/Euro V		RME, Euro V, SCR		HVO, Euro V, SCR		HVO _{HEV} , Euro V, SCR		HVO _{HEV} , Euro VI	
Species	MdEF (mg kg _{fuel} ⁻¹)	Species	MdEF (mg kg _{fuel} ⁻¹)	Species	MdEF (mg kg _{fuel} ⁻¹)	Species	MdEF (mg kg _{fuel} ⁻¹)	Species	MdEF (mg kg _{fuel} ⁻¹)	Species	MdEF (mg kg _{fuel} ⁻¹)
HONO	20.64	HONO	4.92	HONO	12.72	HONO	7.62	HONO	38.96	C ₃ H ₂ O ₂	2.42
HNO ₃	5.29	C ₂ H ₄ O ₂	4.68	HNO ₃	3.24	HNO ₃	2.20	HNCO	14.74	C ₂ H ₄ O ₂	1.23

C ₂ H ₄ O ₂	4.84	HNO ₃	3.48	C ₂ H ₄ O ₂	1.23	C ₂ H ₄ O ₂	1.23	HNO ₃	7.89	C ₂ H ₂ O ₃	0.62
CH ₂ O ₂	1.97	HNCO	0.51	CH ₂ O ₂	0.48	C ₃ H ₆ O ₃	0.14	C ₂ H ₄ O ₂	1.83	C ₈ H ₆ O ₄	0.40
C ₃ H ₆ O ₃	1.79	CH ₂ O ₂	0.30	HNCO	0.15	C ₃ H ₂ O ₂	0.09	CH ₂ O ₂	0.45	C ₆ H ₅ NO ₂	0.31
CH ₄ SO ₃	0.71	C ₂ H ₂ O ₃	0.25	C ₂ H ₂ O ₃	0.05	HNCO	0.08	C ₃ H ₆ O ₃	0.43	HNCO	0.27
HNCO	0.67	C ₃ H ₂ O ₂	0.14	C ₅ H ₈ O ₃	0.03	CH ₂ O ₂	0.02	C ₃ H ₂ O ₂	0.34	C ₃ H ₄ O ₅	0.22
C ₃ H ₄ O ₅	0.37	C ₃ H ₄ O ₂	0.06	CH ₄ SO ₃	0.02	C ₂ H ₂ O ₃	0.02	C ₅ H ₁₀ O ₃	0.16	C ₇ H ₆ O ₃	0.20
C ₂ H ₂ O ₃	0.31	C ₇ H ₆ O ₃	0.05	C ₃ H ₄ O ₂	0.02	C ₃ H ₄ O ₃	0.02	C ₈ H ₆ O ₄	0.12	C ₅ H ₈ O ₃	0.17
C ₄ H ₆ O ₄	0.22	C ₃ H ₈ O ₄	0.05	C ₆ H ₆ N ₂ O ₂	0.01	C ₄ H ₆ O ₄	0.01	C ₅ H ₈ O ₃	0.10	H ₄ N ₂ O ₂ S	0.16

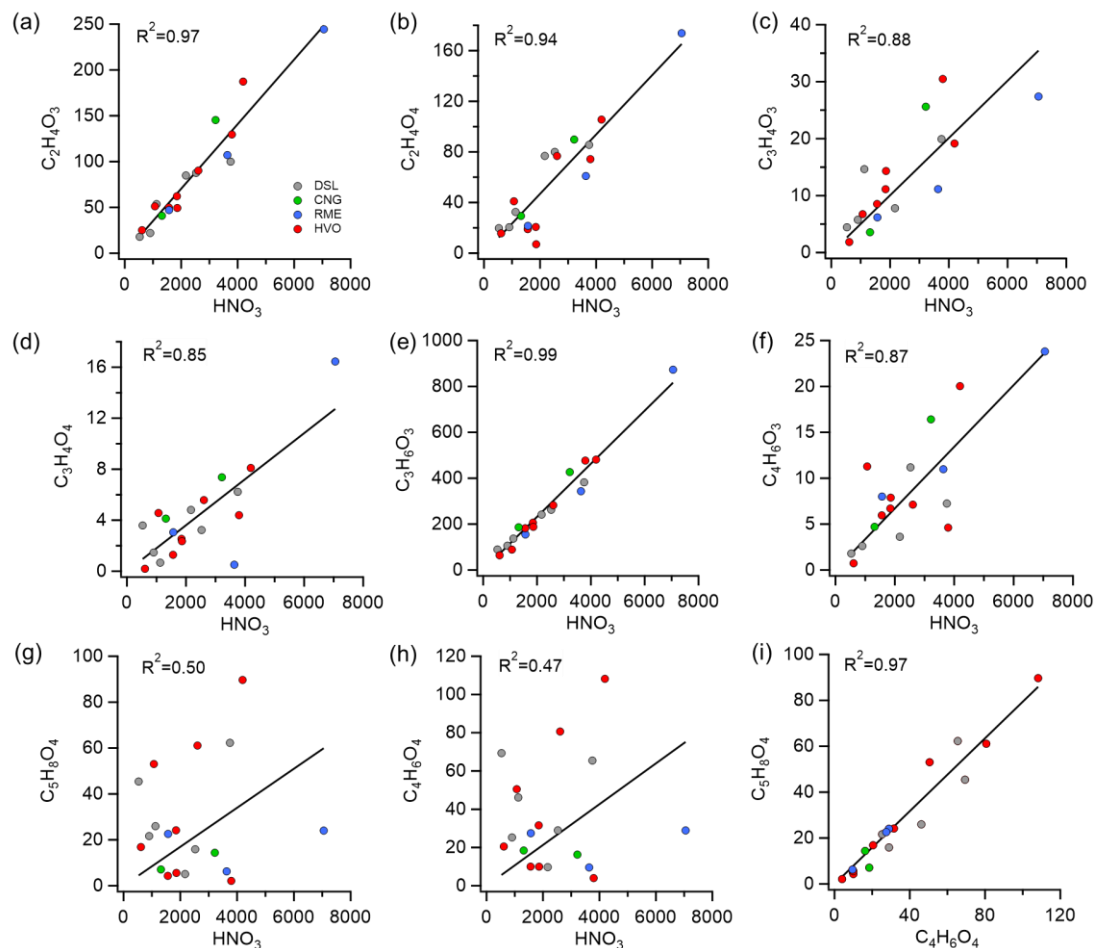
440 ^aDSL, CNG, RME, HVO and HVO_{HFEV}, abbreviations for diesel, compressed natural gas, rapeseed methyl ester, hydrotreated vegetable oil, and hybrid-electric
441 hydrotreated vegetable oil.

442

443

444 3.2.2 Aged gaseous emissions

445 Secondary carboxylic acids were measured following exposure of the exhaust to OH radicals. Figure 5 shows the correlations
446 between ion counts of the most abundant gas-phase organic acids and nitric acid (HNO₃) after oxidation in the Go:PAM. HNO₃
447 serves as an indicator of NO_x oxidation. Most acids exhibited both primary and secondary sources, except for dihydroxyacetic
448 acid (C₂H₄O₄), which was only identified post-aging. The chemical characterization of the aged emissions was conducted on
449 separate occasions using HR-ToF-CIMS, capturing a limited number of buses (N=19). When these buses were categorized by
450 fuel type, the sample size for each category became smaller, constraining statistical comparison across different bus types.
451 Nevertheless, we analyzed the relationship between various chemical species across all buses. Glycolic acid (C₂H₄O₃),
452 dihydroxyacetic acid (C₂H₄O₄), pyruvic acid (C₃H₄O₃), malonic acid (C₃H₄O₄), lactic acid (C₃H₆O₃) and acetoacetic acid
453 (C₄H₆O₃) showed high correlations (R²= 0.85-0.99, Fig. 5a-f) with HNO₃ signals. In contrast, glutaric acid (C₅H₈O₄) and
454 succinic acid (C₄H₆O₄) exhibited poorer correlations with HNO₃, suggesting different formation mechanisms for these two
455 organic acids compared to the others mentioned. Notably, these two acids showed a strong correlation with each other (R²=
456 0.97, Fig. 5i) and both belong to the diacid/hydroxycarbonyl acid families. It is important to note that many of these carboxylic
457 acids can directly participate in secondary PM formation in the atmosphere in the presence of water vapor and a base such as
458 ammonia (Chen et al., 2020; Huang et al., 2018; Hao et al., 2020). This process may significantly contribute to the overall
459 secondary PM yield, reflecting a more complex interplay between gaseous emissions and particulate matter under atmospheric
460 conditions. While most of these small organic acids correlated well with HNO₃, their correlations with EF_{PM:aged} or ΔPM were
461 moderate to weak (R² < 0.6, Figure S4S5). This possibly indicates that the OH-driven formation of these carboxylic acids
462 occurs on a different time scale compared to the production of organic aerosol (Friedman et al., 2017), at least in this Go:PAM
463 experiment. This could also be due to different subsets of hydrocarbon precursors driving the production of organic acids and
464 secondary particle mass. Similarly, Friedman et al. (2017) observed a lack of correlation between organic aerosol and gaseous
465 organic acid concentrations downstream of the flow reactor from a diesel engine, indicating that organic acids may not be
466 reliable tracers for secondary organic aerosol formation from diesel exhaust.



470 Figure 5. Correlations between ion counts of most abundant gas-phase organic acids and HNO_3 (a-h) and correlation between
 471 glutaric acid ($\text{C}_5\text{H}_8\text{O}_4$) and succinic acid ($\text{C}_4\text{H}_6\text{O}_4$) (i) from 19 buses after oxidation in the Go:PAM. Abbreviations: DSL
 472 (diesel), CNG (compressed natural gas), RME (rapeseed methyl ester), HVO (hydrotreated vegetable oil), HVO_{HEV} (hybrid-
 473 electric HVO).

477 3.2.3 Particulate emissions

478 Table 3 displays the top 10 EFs of fresh particle-phase compounds (EF_{fresh}), as characterized by the FIGAERO ToF-CIMS,
 479 alongside their respective aged EFs (EF_{aged}), for Euro V DSL and RME buses. These top 10 EF_{fresh} contributed to over 82% of
 480 the total fresh particulate emissions measured by CIMS. Fresh particulate emissions from DSL buses were predominantly

481 composed of sulfuric acid (H_2SO_4) and nitric acid (HNO_3). Benzene/toluene oxidation products ($\text{C}_7\text{H}_4\text{O}_7$, $\text{C}_7\text{H}_8\text{O}$, $\text{C}_6\text{H}_5\text{NO}_3$,
482 $\text{C}_6\text{H}_5\text{O}$, $\text{C}_7\text{H}_7\text{NO}_3$) also had relatively high EF_{fresh} , aligning with the findings in Le Breton et al. (2019). Similarly, high EF_{fresh}
483 of HNO_3 ($2.5 \text{ mg kg-fuel}^{-1}$) and H_2SO_4 ($0.61 \text{ kg-fuel}^{-1}$) were observed for the RME bus. Additionally, fatty acids, known as
484 main components of unburned rapeseed oil (Usmanov et al., 2015), such as $\text{C}_{18}\text{H}_{34}\text{O}_2$, $\text{C}_{14}\text{H}_{28}\text{O}_2$, $\text{C}_{18}\text{H}_{36}\text{O}_2$, $\text{C}_{16}\text{H}_{32}\text{O}_2$, and
485 $\text{C}_{16}\text{H}_{30}\text{O}_2$, significantly contributed to the identified mass loadings from the RME bus. When comparing the percentage mass
486 observed by CIMS for both DSL and RME fuels in fresh and aged exhaust plumes, the total emission factors measured by
487 CIMS (EF_{CIMS}) were notably lower than the total emission factors measured by the EEPS (EF_{total}). This difference is expected
488 due to the sensitivity of the acetate ionization scheme of CIMS, which efficiently detects oxygenated volatile organic
489 compounds, particularly carboxylic acids and inorganic acids, but has low sensitivity towards hydrocarbons and cannot detect
490 metallic ions and soot. The CIMS measured EF_{fresh} accounted for 10.4% and 5.9% of the fresh EF_{total} measured by the EEPS
491 for DSL and RME, respectively. In aged exhaust, EF_{CIMS} represented a higher percentage of EF_{total} (25.8% for DSL and 17.9%
492 for RME), likely because of an increased proportion of organics with acid groups.

493

494 Table 3. Summary of top 10 EF_{fresh} of PM contributing species with respective EF_{aged} in Euro V DSL and RME emissions.

DSL			RME		
Species	EF_{fresh} ($\text{mg kg}_{\text{fuel}}^{-1}$)	EF_{aged} ($\text{mg kg}_{\text{fuel}}^{-1}$)	Species	EF_{fresh} ($\text{mg kg}_{\text{fuel}}^{-1}$)	EF_{aged} ($\text{mg kg}_{\text{fuel}}^{-1}$)
H_2SO_4	4.8	6.8	HNO_3	2.5	45
HNO_3	3.2	50	$\text{C}_{18}\text{H}_{34}\text{O}_2$	1.2	0.81
$\text{C}_7\text{H}_4\text{O}_7$	1.8	3.8	H_2SO_4	0.61	0.68
HNCO	1.1	1.2	$\text{C}_{14}\text{H}_{28}\text{O}_2$	0.52	0.85
$\text{C}_7\text{H}_8\text{O}$	0.9	7.2	HNCO	0.45	0.089
$\text{C}_3\text{H}_6\text{O}_3$	0.6	23	$\text{C}_{18}\text{H}_{36}\text{O}_2$	0.32	0.046
$\text{C}_6\text{H}_5\text{NO}_3$	0.53	2.6	$\text{C}_{16}\text{H}_{32}\text{O}_2$	0.30	0.18
$\text{C}_4\text{H}_6\text{O}_5$	0.45	0.30	$\text{C}_6\text{H}_5\text{O}_2$	0.12	8.6
$\text{C}_6\text{H}_5\text{O}$	0.26	15.6	$\text{C}_4\text{H}_6\text{O}_4$	0.089	6.3
$\text{C}_7\text{H}_7\text{NO}_3$	0.15	4.6	$\text{C}_{16}\text{H}_{30}\text{O}_2$	0.081	0.012
EF_{total} measured by the EEPS	160.9	1289.8	EF_{total} measured by the EEPS	127.7	1320.6
EF_{CIMS}	16.8	320.1	EF_{CIMS}	7.5	237.2
$\text{EF}_{\text{CIMS}}/\text{EF}_{\text{total}}$ (%)	10.4	25.8	$\text{EF}_{\text{CIMS}}/\text{EF}_{\text{total}}$ (%)	5.9	17.9

495

496

497 4. Conclusion/ atmospheric implications

498 To address the challenges posed by increasing transportation needs, associated greenhouse gas emissions, and related climate
499 change impacts, biofuels have been promoted as a low-carbon alternative to fossil fuels. In 2020, for the 27 Member States of
500 the European Union, 93.2% of the total fuel supply for road transport was derived from fossil fuels, while 6.8% came from
501 biofuels, with Sweden having the highest biofuel share at 23.2% (Vourliotakis and Platsakis, 2022). This study investigated

502 renewable fuels like rapeseed methyl ester (RME), hydrotreated vegetable oil (HVO), and methane (when using biogas) in
503 terms of primary emissions of pollutants and their secondary formation after photochemical aging. DSL buses without a DPF
504 displayed the highest $EF_{PM:Fresh}$, whereas compressed natural gas (CNG) buses emitted the least, with a median $EF_{PM:Fresh}$ below
505 the detection limit. ~~Despite more than an order of magnitude difference in $EF_{PM:Fresh}$ among buses operated using various fuel
506 types, secondary particle formation from the photooxidation of emissions was notable for all 76 buses studied. The median
507 ratio of aged to fresh particle mass emission factors, in ascending order, was diesel (4.0), HVO (6.7), HVO_{HEV} (10.5), RME
508 (10.8), and CNG buses (84). This underscores the importance of considering the potential for forming secondary particle mass
509 in future vehicle emission legislation and in evaluating environmental impacts. The omission of this secondary formation
510 process from current legislation, while important for climate and health reasons, can lead to an incomplete understanding of
511 the potential impact of mobile sources or emission control measures on regional air quality. The inclusion of secondary
512 pollutants in emission regulations is essential for a more comprehensive assessment of their effects. Despite more than an order
513 of magnitude difference in $EF_{PM:Fresh}$ among buses operated with various fuel types, we observed smaller variations in $EF_{PM:Aged}$,
514 suggesting that secondary particle formation is likely influenced by substantial non-fuel-dependent precursor sources such as
515 lubrication oils and/or fuel additives. Recognizing these sources is crucial for refining regulations on hydrocarbon emissions,
516 which could notably enhance SOA control. The median ratios of aged to fresh particle mass emission factors, listed in
517 ascending order, were for diesel (4.0), HVO (6.7), HVO_{HEV} (10.5), RME (10.8), and CNG buses (84), highlighting the
518 significant yet often overlooked contributions of aged/photochemically processed emissions to urban air quality. Furthermore,
519 Zhao et al. (2017) revealed a strongly nonlinear relationship between SOA formation from vehicle exhaust and the ratio of
520 non-methane organic gas to NO_x (NMOG: NO_x). For instance, increasing the NMOG: NO_x from 4 to 10 ppbC/ppb NO_x
521 increased the SOA yield from dilute gasoline vehicle exhaust by a factor of 8, underscoring the importance of integrated
522 emission control policies for NO_x and organic gases for better manage SOA formation. While implementing regulations for
523 secondary particle formation presents significant challenges, these are crucial for a thorough understanding of their impact on
524 regional air quality and health. Our approach to measuring the maximum SOA formation potential—peaking at a
525 photochemical age of approximately 5 equivalent days of atmospheric OH exposure—provides a possible semi-quantitative
526 reference for comparing SOA formation potential across different studies. We acknowledge the limitations of this approach
527 for direct regulatory application and emphasize the need for more precise and comprehensive research to develop a
528 methodologically robust framework that stakeholders can agree upon for systematically assessing the impacts of vehicle on
529 air quality and informing regulatory strategies.~~

530

531 ~~It is important to note that the ambient temperature during this study was relatively low, which does not affect the EF
532 comparison across different buses but should be aware of when comparing these results to studies conducted at significantly
533 higher temperatures. Wang et al. (2017) noted lower particle number EFs in summer compared to winter, potentially due to
534 increased nucleation or condensation at cooler temperatures. Temperature impacts on emissions are significant during cold
535 starts when combustion is inefficient (Nam et al., 2010). Post-warm-up, soot mode particles show little temperature~~

536 sensitivity (Ristimäki et al., 2005). Book et al. (2015) found inconsistent trends in particle emissions from DPF-equipped
537 diesel trucks across various temperatures and driving cycles, suggesting that more research is needed to understand the
538 temperature effects on emissions from different bus types under varied operational conditions.

539

540 Non-regulated chemical species can also have serious negative impacts on air quality and human health. Organic and inorganic
541 acids influence the pH of precipitation and will potentially contribute to acid deposition, affecting ecosystem health.

542 ~~Furthermore, there is a risk that some abatement systems might generate specific compounds. For instance, isocyanic acid~~
543 ~~(HNCO), a byproduct of urea-SCR exhaust systems, has been linked to health issues such as atherosclerosis, cataracts, and~~
544 ~~rheumatoid arthritis (Leslie et al., 2019; Roberts et al., 2011).~~ Furthermore, there is a risk that some abatement systems might
545 generate unintended compounds, such as HNCO from the thermal degradation of urea in SCR systems without sufficient
546 hydrolysis. Additionally, Jathar et al. (2017b) observed substantial direct emissions of HNCO from diesel engines and
547 estimated that ambient concentrations in Los Angeles could vary widely, ranging from 20 to 107 ppt depending on different
548 parameterizations of diesel engine emissions. The persistence of HNCO in the atmosphere, particularly under dry conditions,
549 poses significant health risks. It has been linked to severe outcomes including respiratory and cardiovascular disorders,
550 atherosclerosis, cataracts, and rheumatoid arthritis (Leslie et al., 2019; Roberts et al., 2011). In our study, small monoacids

551 (C₁-C₃) and nitrogen-containing compounds, such as nitrous acid (HONO), nitric acid (HNO₃), and HNCO, dominated the
552 fresh gaseous emissions measured by acetate-CIMS for all Euro V/EEV buses regardless of fuel type, with HVO_{HEV} buses
553 exhibiting the highest emissions. ~~Notably, nitrogen-containing compounds were significantly reduced in Euro VI buses, which~~
554 ~~operated with after-treatment systems incorporating EGR and DPF in addition to SCR-only techniques.~~ Notably, the emission
555 levels of nitrogen-containing compounds were significantly lowered in Euro VI buses, equipped with advanced after-treatment
556 systems that include EGR and DPF technologies in addition to SCR-only techniques. This indicates that transitioning to
557 vehicles equipped with more advanced emission control technologies can be beneficial, even though these technologies may
558 not be specifically designed to target emissions of HONO, HNO₃, and HNCO. Consequently, a detailed evaluation of the
559 environmental and health effects of emerging engine and after-treatment technologies is highly desirable for future
560 considerations. Overall, the extended online chemical characterization of in-use fleet emissions, utilizing advanced techniques
561 like HR-ToF-CIMS, enables the identification of unregulated pollutants, which is crucial for more informed policy decisions
562 and vehicle technology developments.

563

564 ***Data availability.***

565 The data used in this publication are available to the community and can be accessed by request to the corresponding author.

566

567 ***Author contributions.***

568 ÅMH, MLB and QL conducted the measurements. ÅMH designed the project, coordinated the measurements and together
569 with MH and CKC supervised the study. LZ, QL, MLB, CMS and ÅMH carried out the data analysis. LZ, QL, JZY, MH,
570 ÅMH and CKC prepared the manuscript. All co-authors contributed to the discussion and the interpretation of the results.

571

572 *Competing interests.*

573 The authors declare that they have no known competing financial interests or personal relationships that could have appeared
574 to influence the work reported in this paper.

575

576 *Acknowledgments.*

577 This work was financed by VINNOVA, Sweden's Innovation Agency (2013-03058) and Formas (2020-1907) and was an
578 initiative within the framework programme "Photochemical smog in China" financed by the Swedish Research Council (639-
579 2013-6917). Chak K. Chan would like to acknowledge the support of the National Natural Science Foundation of China
580 (project no. 41675117 and 41875142).

581 **References**

- 582 Aljawhary, D., Lee, A. K. Y., and Abbatt, J. P. D.: High-resolution chemical ionization mass spectrometry (ToF-CIMS): application to study
583 SOA composition and processing, *Atmospheric Measurement Techniques*, 6, 3211-3224, 10.5194/amt-6-3211-2013, 2013.
- 584 Arnold, F., Pirjola, L., Ronkko, T., Reichl, U., Schlager, H., Lahde, T., Heikkila, J., and Keskinen, J.: First online measurements of sulfuric
585 acid gas in modern heavy-duty diesel engine exhaust: implications for nanoparticle formation, *Environmental science & technology*, 46,
586 11227-11234, 2012.
- 587 Bernhard, A. M., Peitz, D., Elsener, M., Wokaun, A., and Kröcher, O.: Hydrolysis and thermolysis of urea and its decomposition byproducts
588 biuret, cyanuric acid and melamine over anatase TiO₂, *Applied Catalysis B: Environmental*, 115, 129-137, 2012.
- 589 Book, E. K., Snow, R., Long, T., Fang, T., and Baldauf, R.: Temperature effects on particulate emissions from DPF-equipped diesel trucks
590 operating on conventional and biodiesel fuels, *Journal of the Air & Waste Management Association*, 65, 751-758, 2015.
- 591 Brady, J. M., Crisp, T. A., Collier, S., Kuwayama, T., Forestieri, S. D., Perraud, V., Zhang, Q., Kleeman, M. J., Cappa, C. D., and Bertram,
592 T. H.: Real-time emission factor measurements of isocyanic acid from light duty gasoline vehicles, *Environ Sci Technol*, 48, 11405-11412,
593 10.1021/es504354p, 2014.
- 594 Bruns, E., El Haddad, I., Keller, A., Klein, F., Kumar, N., Pieber, S., Corbin, J., Slowik, J., Brune, W., and Baltensperger, U.: Inter-
595 comparison of laboratory smog chamber and flow reactor systems on organic aerosol yield and composition, *Atmospheric Measurement*
596 *Techniques*, 8, 2315-2332, 2015.
- 597 Chen, L., Bao, Z., Wu, X., Li, K., Han, L., Zhao, X., Zhang, X., Wang, Z., Azzi, M., and Cen, K.: The effects of humidity and ammonia on
598 the chemical composition of secondary aerosols from toluene/NO_x photo-oxidation, *Science of The Total Environment*, 728, 138671, 2020.
- 599 Chirico, R., DeCarlo, P., Heringa, M., Tritscher, T., Richter, R., Prévôt, A., Dommen, J., Weingartner, E., Wehrle, G., and Gysel, M.: Impact
600 of aftertreatment devices on primary emissions and secondary organic aerosol formation potential from in-use diesel vehicles: results from
601 smog chamber experiments, *Atmospheric Chemistry & Physics*, 10, 11545-11563, 2010.
- 602 Corrêa, S. M., and Arbilla, G.: Mercaptans emissions in diesel and biodiesel exhaust, *Atmospheric Environment*, 42, 6721-6725, 2008.
- 603 Crisp, T. A., Brady, J. M., Cappa, C. D., Collier, S., Forestieri, S. D., Kleeman, M. J., Kuwayama, T., Lerner, B. M., Williams, E. J., and
604 Zhang, Q.: On the primary emission of formic acid from light duty gasoline vehicles and ocean-going vessels, *Atmospheric Environment*,
605 98, 426-433, 2014.
- 606 Deng, W., Hu, Q., Liu, T., Wang, X., Zhang, Y., Song, W., Sun, Y., Bi, X., Yu, J., Yang, W., Huang, X., Zhang, Z., Huang, Z., He, Q.,
607 Mellouki, A., and George, C.: Primary particulate emissions and secondary organic aerosol (SOA) formation from idling diesel vehicle
608 exhaust in China, *Sci Total Environ*, 593-594, 462-469, 10.1016/j.scitotenv.2017.03.088, 2017.
- 609 Edwards, R., Mahieu, V., Griesemann, J.-C., Larivé, J.-F., and Rickeard, D. J.: Well-to-wheels analysis of future automotive fuels and
610 powertrains in the European context, *SAE Technical Paper0148-7191*, 2004.

611 Emanuelsson, E. U., Hallquist, M., Kristensen, K., Glasius, M., Bohn, B., Fuchs, H., Kammer, B., Kiendler-Scharr, A., Nehr, S., and Rubach,
612 F.: Formation of anthropogenic secondary organic aerosol (SOA) and its influence on biogenic SOA properties, *Atmospheric Chemistry and*
613 *Physics*, 13, 2837-2855, 2013.

614 Energimyndigheten: Energy in Sweden 2021 – An Overview, 2021.

615 Fitzmaurice, H. L., and Cohen, R. C.: A method for using stationary networks to observe long-term trends of on-road emission factors of
616 primary aerosol from heavy-duty vehicles, *Atmospheric Chemistry and Physics*, 22, 15403-15411, 2022.

617 Friedman, B., Link, M. F., Fulgham, S. R., Brophy, P., Galang, A., Brune, W. H., Jathar, S. H., and Farmer, D. K.: Primary and Secondary
618 Sources of Gas-Phase Organic Acids from Diesel Exhaust, *Environ Sci Technol*, 51, 10872-10880, 10.1021/acs.est.7b01169, 2017.

619 Gentner, D. R., Jathar, S. H., Gordon, T. D., Bahreini, R., Day, D. A., El Haddad, I., Hayes, P. L., Pieber, S. M., Platt, S. M., and de Gouw,
620 J.: Review of urban secondary organic aerosol formation from gasoline and diesel motor vehicle emissions, *Environmental science &*
621 *technology*, 51, 1074-1093, 2017.

622 Ghadimi, S., Zhu, H., Durbin, T. D., Cocker III, D. R., and Karavalakis, G.: Exceedances of Secondary Aerosol Formation from In-Use
623 Natural Gas Heavy-Duty Vehicles Compared to Diesel Heavy-Duty Vehicles, *Environmental Science & Technology*, 57, 19979-19989,
624 2023.

625 Giechaskiel, B., Riccobono, F., Vlachos, T., Mendoza-Villafuerte, P., Suarez-Bertoa, R., Fontaras, G., Bonnel, P., and Weiss, M.: Vehicle
626 emission factors of solid nanoparticles in the laboratory and on the road using portable emission measurement systems (PEMS), *Frontiers in*
627 *Environmental Science*, 3, 82, 2015.

628 Gordon, T. D., Presto, A. A., May, A. A., Nguyen, N. T., Lipsky, E. M., Donahue, N. M., Gutierrez, A., Zhang, M., Maddox, C., Rieger, P.,
629 Chattopadhyay, S., Maldonado, H., Maricq, M. M., and Robinson, A. L.: Secondary organic aerosol formation exceeds primary particulate
630 matter emissions for light-duty gasoline vehicles, *Atmospheric Chemistry and Physics*, 14, 4661-4678, 10.5194/acp-14-4661-2014, 2014a.

631 Gordon, T. D., Presto, A. A., Nguyen, N. T., Robertson, W. H., Na, K., Sahay, K. N., Zhang, M., Maddox, C., Rieger, P., Chattopadhyay,
632 S., Maldonado, H., Maricq, M. M., and Robinson, A. L.: Secondary organic aerosol production from diesel vehicle exhaust: impact of
633 aftertreatment, fuel chemistry and driving cycle, *Atmospheric Chemistry and Physics*, 14, 4643-4659, 10.5194/acp-14-4643-2014, 2014b.

634 Guerreiro, C. B., Foltescu, V., and De Leeuw, F.: Air quality status and trends in Europe, *Atmospheric environment*, 98, 376-384, 2014.

635 Hak, C. S., Hallquist, M., Ljungstrom, E., Svane, M., and Pettersson, J. B. C.: A new approach to in-situ determination of roadside particle
636 emission factors of individual vehicles under conventional driving conditions, *Atmospheric Environment*, 43, 2481-2488,
637 10.1016/j.atmosenv.2009.01.041, 2009.

638 Hallquist, A. M., Jerksjo, M., Fallgren, H., Westerlund, J., and Sjodin, A.: Particle and gaseous emissions from individual diesel and CNG
639 buses, *Atmospheric Chemistry and Physics*, 13, 5337-5350, 10.5194/acp-13-5337-2013, 2013.

640 Hallquist, M., Wenger, J. C., Baltensperger, U., Rudich, Y., Simpson, D., Claeys, M., Dommen, J., Donahue, N., George, C., and Goldstein,
641 A.: The formation, properties and impact of secondary organic aerosol: current and emerging issues, *Atmospheric chemistry and physics*, 9,
642 5155-5236, 2009.

643 Hao, L., Kari, E., Leskinen, A., Worsnop, D. R., and Virtanen, A.: Direct contribution of ammonia to α -pinene secondary organic
644 aerosol formation, *Atmospheric Chemistry and Physics*, 20, 14393-14405, 2020.

645 Hassaneen, A., Munack, A., Ruschel, Y., Schroeder, O., and Krahl, J.: Fuel economy and emission characteristics of Gas-to-Liquid (GTL)
646 and Rapeseed Methyl Ester (RME) as alternative fuels for diesel engines, *Fuel*, 97, 125-130, 2012.

647 Huang, M., Xu, J., Cai, S., Liu, X., Hu, C., Gu, X., Zhao, W., Fang, L., and Zhang, W.: Chemical analysis of particulate products of aged 1,
648 3, 5-trimethylbenzene secondary organic aerosol in the presence of ammonia, *Atmospheric Pollution Research*, 9, 146-155, 2018.

649 Janhäll, S., and Hallquist, M.: A novel method for determination of size-resolved, submicrometer particle traffic emission factors,
650 *Environmental Science & Technology*, 39, 7609-7615, <http://doi.org/10.1021/es048208y>, 2005.

651 Jathar, S. H., Friedman, B., Galang, A. A., Link, M. F., Brophy, P., Volckens, J., Eluri, S., and Farmer, D. K.: Linking load, fuel, and
652 emission controls to photochemical production of secondary organic aerosol from a diesel engine, *Environmental science & technology*, 51,
653 1377-1386, 2017a.

654 Jathar, S. H., Heppding, C., Link, M. F., Farmer, D. K., Akherati, A., Kleeman, M. J., de Gouw, J. A., Veres, P. R., and Roberts, J. M.:
655 Investigating diesel engines as an atmospheric source of isocyanic acid in urban areas, *Atmospheric Chemistry and Physics*, 17, 8959-8970,
656 10.5194/acp-17-8959-2017, 2017b.

657 Jezek, I., Drinovec, L., Ferrero, L., Carriero, M., and Mocnik, G.: Determination of car on-road black carbon and particle number emission
658 factors and comparison between mobile and stationary measurements, *Atmospheric Measurement Techniques*, 8, 43-55, 10.5194/amt-8-43-
659 2015, 2015.

660 Kang, E., Root, M. J., Toohey, D. W., and Brune, W. H.: Introducing the concept of Potential Aerosol Mass (PAM), *Atmospheric Chemistry*
661 *and Physics*, 7, 5727-5744, DOI 10.5194/acp-7-5727-2007, 2007.

662 Kawamura, K., Ng, L. L., and Kaplan, I. R.: Determination of organic acids (C1-C10) in the atmosphere, motor exhausts, and engine oils,
663 *Environmental science & technology*, 19, 1082-1086, 1985.

664 Kawamura, K., and Kaplan, I. R.: Motor exhaust emissions as a primary source for dicarboxylic acids in Los Angeles ambient air,
665 *Environmental science & technology*, 21, 105-110, 1987.

666 Kirchstetter, T. W., Harley, R. A., and Littlejohn, D.: Measurement of nitrous acid in motor vehicle exhaust, *Environmental science &*
667 *technology*, 30, 2843-2849, 1996.

668 Kroll, J. H., Smith, J. D., Che, D. L., Kessler, S. H., Worsnop, D. R., and Wilson, K. R.: Measurement of fragmentation and functionalization
669 pathways in the heterogeneous oxidation of oxidized organic aerosol, *Physical Chemistry Chemical Physics*, 11, 8005-8014, 2009.

670 Kuittinen, N., McCaffery, C., Peng, W., Zimmerman, S., Roth, P., Simonen, P., Karjalainen, P., Keskinen, J., Cocker, D. R., and Durbin, T.
671 D.: Effects of driving conditions on secondary aerosol formation from a GDI vehicle using an oxidation flow reactor, *Environmental*
672 *Pollution*, 282, 117069, 2021.

673 Kurtenbach, R., Becker, K., Gomes, J., Kleffmann, J., Lörzer, J., Spittler, M., Wiesen, P., Ackermann, R., Geyer, A., and Platt, U.:
674 Investigations of emissions and heterogeneous formation of HONO in a road traffic tunnel, *Atmospheric Environment*, 35, 3385-3394, 2001.

675 Kwak, J. H., Kim, H. S., Lee, J. H., and Lee, S. H.: On-Road Chasing Measurement of Exhaust Particle Emissions from Diesel, Cng Lpg
676 and Dme-Fueled Vehicles Using a Mobile Emission Laboratory, *International Journal of Automotive Technology*, 15, 543-551,
677 <http://doi.org/10.1007/s12239-014-0057-z>, 2014.

678 Lambe, A., Ahern, A., Williams, L., Slowik, J., Wong, J., Abbatt, J., Brune, W., Ng, N., Wright, J., and Croasdale, D.: Characterization of
679 aerosol photooxidation flow reactors: heterogeneous oxidation, secondary organic aerosol formation and cloud condensation nuclei activity
680 measurements, *Atmospheric Measurement Techniques*, 4, 445-461, 2011.

681 Le Breton, M., Wang, Y., Hallquist, Å. M., Pathak, R. K., Zheng, J., Yang, Y., Shang, D., Glasius, M., Bannan, T. J., and Liu, Q.: Online
682 gas-and particle-phase measurements of organosulfates, organosulfonates and nitrooxy organosulfates in Beijing utilizing a FIGAERO ToF-
683 CIMS, *Atmospheric Chemistry and Physics*, 18, 10355-10371, 2018.

684 Le Breton, M., Psichoudaki, M., Hallquist, M., Watne, Å., Lutz, A., and Hallquist, Å.: Application of a FIGAERO ToF CIMS for on-line
685 characterization of real-world fresh and aged particle emissions from buses, *Aerosol Science and Technology*, 53, 244-259, 2019.

686 Leslie, M. D., Ridoli, M., Murphy, J. G., and Borduas-Dedekind, N.: Isocyanic acid (HNCO) and its fate in the atmosphere: a review,
687 *Environmental Science: Processes & Impacts*, 21, 793-808, 2019.

688 Li, T., Wang, Z., Yuan, B., Ye, C., Lin, Y., Wang, S., Yuan, Z., Zheng, J., and Shao, M.: Emissions of carboxylic acids, hydrogen cyanide
689 (HCN) and isocyanic acid (HNCO) from vehicle exhaust, *Atmospheric Environment*, 247, 118218, 2021.

690 Liao, K., Chen, Q., Liu, Y., Li, Y. J., Lambe, A. T., Zhu, T., Huang, R.-J., Zheng, Y., Cheng, X., and Miao, R.: Secondary Organic Aerosol
691 Formation of Fleet Vehicle Emissions in China: Potential Seasonality of Spatial Distributions, *Environmental Science & Technology*, 2021a.

692 Liao, K., Chen, Q., Liu, Y., Li, Y. J., Lambe, A. T., Zhu, T., Huang, R.-J., Zheng, Y., Cheng, X., and Miao, R.: Secondary organic aerosol
693 formation of fleet vehicle emissions in China: Potential seasonality of spatial distributions, *Environmental Science & Technology*, 55, 7276-
694 7286, 2021b.

695 Liao, S., Zhang, J., Yu, F., Zhu, M., Liu, J., Ou, J., Dong, H., Sha, Q., Zhong, Z., and Xie, Y.: High gaseous nitrous acid (HONO) emissions
696 from light-duty diesel vehicles, *Environmental science & technology*, 55, 200-208, 2020.

697 Link, M. F., Friedman, B., Fulgham, R., Brophy, P., Galang, A., Jathar, S. H., Veres, P., Roberts, J. M., and Farmer, D. K.: Photochemical
698 processing of diesel fuel emissions as a large secondary source of isocyanic acid (HNCO), *Geophysical Research Letters*, 43, 4033-4041,
699 10.1002/2016gl068207, 2016.

700 Liu, Q., Hallquist, Å. M., Fallgren, H., Jerksjö, M., Jutterström, S., Salberg, H., Hallquist, M., Le Breton, M., Pei, X., and Pathak, R. K.:
701 Roadside assessment of a modern city bus fleet: Gaseous and particle emissions, *Atmospheric Environment: X*, 3, 100044, 2019a.

702 Liu, S., Thompson, S. L., Stark, H., Ziemann, P. J., and Jimenez, J. L.: Gas-phase carboxylic acids in a university classroom: Abundance,
703 variability, and sources, *Environmental Science & Technology*, 51, 5454-5463, 2017.

704 Liu, T., Wang, X., Deng, W., Hu, Q., Ding, X., Zhang, Y., He, Q., Zhang, Z., Lu, S., Bi, X., Chen, J., and Yu, J.: Secondary organic aerosol
705 formation from photochemical aging of light-duty gasoline vehicle exhausts in a smog chamber, *Atmospheric Chemistry and Physics*, 15,
706 9049-9062, 10.5194/acp-15-9049-2015, 2015.

707 Liu, T., Zhou, L., Liu, Q., Lee, B. P., Yao, D., Lu, H., Lyu, X., Guo, H., and Chan, C. K.: Secondary Organic Aerosol Formation from Urban
708 Roadside Air in Hong Kong, *Environ Sci Technol*, 53, 3001-3009, 10.1021/acs.est.8b06587, 2019b.

709 Lopez-Hilfiker, F., Mohr, C., Ehn, M., Rubach, F., Kleist, E., Wildt, J., Mentel, T. F., Carrasquillo, A., Daumit, K., and Hunter, J.: Phase
710 partitioning and volatility of secondary organic aerosol components formed from α -pinene ozonolysis and OH oxidation: the importance of
711 accretion products and other low volatility compounds, *Atmospheric chemistry and physics*, 15, 7765-7776, 2015.

712 Lopez-Hilfiker, F. D., Mohr, C., Ehn, M., Rubach, F., Kleist, E., Wildt, J., Mentel, T. F., Lutz, A., Hallquist, M., Worsnop, D., and Thornton,
713 J. A.: A novel method for online analysis of gas and particle composition: description and evaluation of a Filter Inlet for Gases and AEROSols
714 (FIGAERO), *Atmospheric Measurement Techniques*, 7, 983-1001, 10.5194/amt-7-983-2014, 2014.

715 Martinet, S., Liu, Y., Louis, C., Tassel, P., Perret, P., Chaumont, A., and Andre, M.: Euro 6 unregulated pollutant characterization and
716 statistical analysis of after-treatment device and driving-condition impact on recent passenger-car emissions, *Environmental Science &*
717 *Technology*, 51, 5847-5855, 2017.

718 May, A. A., Nguyen, N. T., Presto, A. A., Gordon, T. D., Lipsky, E. M., Karve, M., Gutierrez, A., Robertson, W. H., Zhang, M., Brandow,
719 C., Chang, O., Chen, S. Y., Cicero-Fernandez, P., Dinkins, L., Fuentes, M., Huang, S. M., Ling, R., Long, J., Maddox, C., Massetti, J.,
720 McCauley, E., Miguel, A., Na, K., Ong, R., Pang, Y. B., Rieger, P., Sax, T., Truong, T., Vo, T., Chattopadhyay, S., Maldonado, H., Maricq,

721 M. M., and Robinson, A. L.: Gas- and particle-phase primary emissions from in-use, on-road gasoline and diesel vehicles, *Atmospheric*
722 *Environment*, 88, 247-260, 10.1016/j.atmosenv.2014.01.046, 2014.

723 Millet, D. B., Baasandorj, M., Farmer, D. K., Thornton, J. A., Baumann, K., Brophy, P., Chaliyakunnel, S., de Gouw, J. A., Graus, M., and
724 Hu, L.: A large and ubiquitous source of atmospheric formic acid, *Atmospheric Chemistry and Physics*, 15, 6283-6304, 2015.

725 Mohr, C., Lopez-Hilfiker, F. D., Yli-Juuti, T., Heitto, A., Lutz, A., Hallquist, M., D'Ambro, E. L., Rissanen, M. P., Hao, L., and
726 Schobesberger, S.: Ambient observations of dimers from terpene oxidation in the gas phase: Implications for new particle formation and
727 growth, *Geophysical Research Letters*, 44, 2958-2966, 2017.

728 Nakashima, Y., and Kondo, Y.: Nitrous acid (HONO) emission factors for diesel vehicles determined using a chassis dynamometer, *Science*
729 *of The Total Environment*, 806, 150927, 2022.

730 Nam, E., Kishan, S., Baldauf, R. W., Fulper, C. R., Sabisch, M., and Warila, J.: Temperature effects on particulate matter emissions from
731 light-duty, gasoline-powered motor vehicles, *Environmental science & technology*, 44, 4672-4677, 2010.

732 Nordin, E. Z., Eriksson, A. C., Roldin, P., Nilsson, P. T., Carlsson, J. E., Kajos, M. K., Hellen, H., Wittbom, C., Rissler, J., Londahl, J.,
733 Swietlicki, E., Svenningsson, B., Bohgard, M., Kulmala, M., Hallquist, M., and Pagels, J. H.: Secondary organic aerosol formation from
734 idling gasoline passenger vehicle emissions investigated in a smog chamber, *Atmospheric Chemistry and Physics*, 13, 6101-6116,
735 10.5194/acp-13-6101-2013, 2013.

736 Ortega, A. M., Hayes, P. L., Peng, Z., Palm, B. B., Hu, W., Day, D. A., Li, R., Cubison, M. J., Brune, W. H., and Graus, M.: Real-time
737 measurements of secondary organic aerosol formation and aging from ambient air in an oxidation flow reactor in the Los Angeles area,
738 *Atmospheric Chemistry and Physics*, 16, 7411-7433, 2016.

739 Palm, B. B., Campuzano-Jost, P., Ortega, A. M., Day, D. A., Kaser, L., Jud, W., Karl, T., Hansel, A., Hunter, J. F., and Cross, E. S.: In situ
740 secondary organic aerosol formation from ambient pine forest air using an oxidation flow reactor, *Atmospheric Chemistry and Physics*, 16,
741 2943-2970, 2016.

742 Paulot, F., Wunch, D., Crounse, J. D., Toon, G., Millet, D. B., DeCarlo, P. F., Vigouroux, C., Deutscher, N. M., González Abad, G., and
743 Notholt, J.: Importance of secondary sources in the atmospheric budgets of formic and acetic acids, *Atmospheric Chemistry and Physics*,
744 11, 1989-2013, 2011.

745 Pflaum, H., Hofmann, P., Geringer, B., and Weissel, W.: Potential of hydrogenated vegetable oil (HVO) in a modern diesel engine, *SAE*
746 *Technical Paper0148-7191*, 2010.

747 Pirjola, L., Karl, M., Rönkkö, T., and Arnold, F.: Model studies of volatile diesel exhaust particle formation: are organic vapours involved
748 in nucleation and growth?, *Atmospheric Chemistry and Physics*, 15, 10435-10452, 2015.

749 Pirjola, L., Dittrich, A., Niemi, J. V., Saarikoski, S., Timonen, H., Kuuluvainen, H., Jarvinen, A., Kousa, A., Ronkko, T., and Hillamo, R.:
750 Physical and Chemical Characterization of Real-World Particle Number and Mass Emissions from City Buses in Finland, *Environ Sci*
751 *Technol*, 50, 294-304, <http://doi.org/10.1021/acs.est.5b04105>, 2016.

752 Platt, S. M., El Haddad, I., Zardini, A. A., Clairotte, M., Astorga, C., Wolf, R., Slowik, J. G., Temime-Roussel, B., Marchand, N., Jezek, I.,
753 Drinovec, L., Mocnik, G., Mohler, O., Richter, R., Barmet, P., Bianchi, F., Baltensperger, U., and Prevot, A. S. H.: Secondary organic aerosol
754 formation from gasoline vehicle emissions in a new mobile environmental reaction chamber, *Atmospheric Chemistry and Physics*, 13, 9141-
755 9158, 10.5194/acp-13-9141-2013, 2013.

756 Preble, C. V., Dallmann, T. R., Kreisberg, N. M., Hering, S. V., Harley, R. A., and Kirchstetter, T. W.: Effects of Particle Filters and Selective
757 Catalytic Reduction on Heavy-Duty Diesel Drayage Truck Emissions at the Port of Oakland, *Environmental Science & Technology*, 49,
758 8864-8871, 10.1021/acs.est.5b01117, 2015.

759 Ristimäki, J., Keskinen, J., Virtanen, A., Maricq, M., and Aakko, P.: Cold temperature PM emissions measurement: Method evaluation and
760 application to light duty vehicles, *Environmental science & technology*, 39, 9424-9430, 2005.

761 Roberts, J. M., Veres, P. R., Cochran, A. K., Warneke, C., Burling, I. R., Yokelson, R. J., Lerner, B., Gilman, J. B., Kuster, W. C., and Fall,
762 R.: Isocyanic acid in the atmosphere and its possible link to smoke-related health effects, *Proceedings of the National Academy of Sciences*,
763 108, 8966-8971, 2011.

764 Saliba, G., Saleh, R., Zhao, Y., Presto, A. A., Lambe, A. T., Frodin, B., Sardar, S., Maldonado, H., Maddox, C., and May, A. A.: Comparison
765 of gasoline direct-injection (GDI) and port fuel injection (PFI) vehicle emissions: emission certification standards, cold-start, secondary
766 organic aerosol formation potential, and potential climate impacts, *Environmental science & technology*, 51, 6542-6552, 2017.

767 Simonen, P., Saukko, E., Karjalainen, P., Timonen, H., Bloss, M., Aakko-Saksa, P., Rönkkö, T., Keskinen, J., and Dal Maso, M.: A new
768 oxidation flow reactor for measuring secondary aerosol formation of rapidly changing emission sources, *Atmospheric Measurement*
769 *Techniques*, 10, 1519-1537, 2017.

770 Suarez-Bertoa, R., and Astorga, C.: Isocyanic acid and ammonia in vehicle emissions, *Transportation Research Part D: Transport and*
771 *Environment*, 49, 259-270, 2016.

772 Tkacik, D. S., Lambe, A. T., Jathar, S., Li, X., Presto, A. A., Zhao, Y. L., Blake, D., Meinardi, S., Jayne, J. T., Croteau, P. L., and Robinson,
773 A. L.: Secondary Organic Aerosol Formation from in-Use Motor Vehicle Emissions Using a Potential Aerosol Mass Reactor, *Environmental*
774 *Science & Technology*, 48, 11235-11242, 10.1021/es502239v, 2014.

775 Tong, Z., Li, Y., Lin, Q., Wang, H., Zhang, S., Wu, Y., and Zhang, K. M.: Uncertainty investigation of plume-chasing method for measuring
776 on-road NOx emission factors of heavy-duty diesel vehicles, *Journal of hazardous materials*, 424, 127372, 2022.

777 Usmanov, R. A., Mazanov, S. V., Gabitova, A. R., Miftakhova, L. K., Gumerov, F. M., Musin, R. Z., and Abdulagatov, I. M.: The effect of
778 fatty acid ethyl esters concentration on the kinematic viscosity of biodiesel fuel, *Journal of Chemical & Engineering Data*, 60, 3404-3413,
779 2015.

780 Vogt, R., Scheer, V., Casati, R., and Benter, T.: On-road measurement of particle emission in the exhaust plume of a diesel passenger car,
781 *Environmental science & technology*, 37, 4070-4076, 2003.

782 Vourliotakis, G., and Platsakis, O.: ETC CM report 2022/02: Greenhouse gas intensities of transport fuels in the EU in 2020 - Monitoring
783 under the Fuel Quality Directive, European Topic Centre on Climate change mitigation, 2022.

784 Wang, H., Wu, Y., Zhang, K. M., Zhang, S., Baldauf, R. W., Snow, R., Deshmukh, P., Zheng, X., He, L., and Hao, J.: Evaluating mobile
785 monitoring of on-road emission factors by comparing concurrent PEMS measurements, *Science of the Total Environment*, 736, 139507,
786 2020.

787 Wang, J. M., Jeong, C.-H., Zimmerman, N., Healy, R. M., Hilker, N., and Evans, G. J.: Real-world emission of particles from vehicles:
788 volatility and the effects of ambient temperature, *Environmental Science & Technology*, 51, 4081-4090, 2017.

789 Wang, Z., Nicholls, S. J., Rodriguez, E. R., Kumm, O., Hörkö, S., Barnard, J., Reynolds, W. F., Topol, E. J., DiDonato, J. A., and Hazen,
790 S. L.: Protein carbamylation links inflammation, smoking, uremia and atherogenesis, *Nature medicine*, 13, 1176-1184, 2007.

791 Watne, A. K., Psychoudaki, M., Ljungstrom, E., Le Breton, M., Hallquist, M., Jerksjö, M., Fallgren, H., Jutterstrom, S., and Hallquist, A.
792 M.: Fresh and Oxidized Emissions from In-Use Transit Buses Running on Diesel, Biodiesel, and CNG, *Environ Sci Technol*, 52, 7720-7728,
793 <https://doi.org/10.1021/acs.est.8b01394>, 2018.

794 Wentzell, J. J., Liggio, J., Li, S. M., Vlasenko, A., Staebler, R., Lu, G., Poitras, M. J., Chan, T., and Brook, J. R.: Measurements of gas phase
795 acids in diesel exhaust: a relevant source of HNCO?, *Environ Sci Technol*, 47, 7663-7671, 10.1021/es401127j, 2013.

796 Yao, D., Guo, H., Lyu, X., Lu, H., and Huo, Y.: Secondary organic aerosol formation at an urban background site on the coastline of South
797 China: Precursors and aging processes, *Environmental Pollution*, 309, 119778, 2022.

798 Yao, X., Fang, M., and Chan, C. K.: Size distributions and formation of dicarboxylic acids in atmospheric particles, *Atmospheric*
799 *Environment*, 36, 2099-2107, 2002.

800 Yuan, B., Veres, P., Warneke, C., Roberts, J., Gilman, J., Koss, A., Edwards, P., Graus, M., Kuster, W., and Li, S.-M.: Investigation of
801 secondary formation of formic acid: urban environment vs. oil and gas producing region, *Atmospheric Chemistry and Physics*, 15, 1975-
802 1993, 2015.

803 Zervas, E., Montagne, X., and Lahaye, J.: C1–C5 organic acid emissions from an SI engine: Influence of fuel and air/fuel equivalence ratio,
804 *Environmental science & technology*, 35, 2746-2751, 2001a.

805 Zervas, E., Montagne, X., and Lahaye, J.: Emission of specific pollutants from a compression ignition engine. Influence of fuel
806 hydrotreatment and fuel/air equivalence ratio, *Atmospheric Environment*, 35, 1301-1306, 2001b.

807 Zhang, R., Suh, I., Zhao, J., Zhang, D., Fortner, E. C., Tie, X., Molina, L. T., and Molina, M. J.: Atmospheric new particle formation
808 enhanced by organic acids, *Science*, 304, 1487-1490, 2004.

809 Zhao, Y., Saleh, R., Saliba, G., Presto, A. A., Gordon, T. D., Drozd, G. T., Goldstein, A. H., Donahue, N. M., and Robinson, A. L.: Reducing
810 secondary organic aerosol formation from gasoline vehicle exhaust, *Proceedings of the National Academy of Sciences*, 114, 6984-6989,
811 2017.

812 Zhao, Y., Lambe, A. T., Saleh, R., Saliba, G., and Robinson, A. L.: Secondary Organic Aerosol Production from Gasoline Vehicle Exhaust:
813 Effects of Engine Technology, Cold Start, and Emission Certification Standard, *Environ Sci Technol*, 52, 1253-1261,
814 <https://doi.org/10.1021/acs.est.7b05045>, 2018.

815 Zhou, L., Hallquist, Å. M., Hallquist, M., Salvador, C. M., Gaita, S. M., Sjödin, Å., Jerksjö, M., Salberg, H., Wängberg, I., and Mellqvist,
816 J.: A transition of atmospheric emissions of particles and gases from on-road heavy-duty trucks, *Atmospheric Chemistry and Physics*, 20,
817 1701-1722, 2020.

818 Zhou, L., Salvador, C. M., Priestley, M., Hallquist, M., Liu, Q., Chan, C. K., and Hallquist, Å. M.: Emissions and secondary formation of
819 air pollutants from modern heavy-duty trucks in real-world traffic—chemical characteristics using on-line mass spectrometry, *Environmental*
820 *Science & Technology*, 55, 14515-14525, 2021.

821